The Journal of Chemical Physics

RESEARCH ARTICLE | FEBRUARY 13 2024

Valence shell electronically excited states of norbornadiene and quadricyclane

Joseph C. Cooper; David M. P. Holland ; Rebecca A. Ingle ; Matteo Bonanomi; Davide Facciala ; Nelson De Oliveira ; Abdul R. Abid ; Julien Bachmann ; Surjendu Bhattacharyya ; Kurtis Borne ; Michael Bosch ; Martin Centurion ; Keyu Chen ; Ruaridh J. G. Forbes ; Huynh V. S. Lam ; Asami Odate ; Artem Rudenko ; Anbu S. Venkatachalam ; Caterina Vozzi ; Enliang Wang ; Peter M. Weber ; Michael N. R. Ashfold ; Adam Kirrander ; Daniel Rolles

Check for updates

J. Chem. Phys. 160, 064305 (2024)
https://doi.org/10.1063/5.0187707
CHORUS

View Online
Export Citation

Articles You May Be Interested In

High-level studies of the ionic states of norbornadiene and quadricyclane, including analysis of new experimental photoelectron spectra by configuration interaction and coupled cluster calculations

J. Chem. Phys. (November 2020)

High-level studies of the singlet states of quadricyclane, including analysis of a new experimental vacuum ultraviolet absorption spectrum by configuration interaction and density functional calculations

J. Chem. Phys. (June 2023)

Evaluation of tight-binding DFT performance for the description of organic photochromes properties

J. Chem. Phys. (February 2023)

28 February 2025 10:38:23

Nanotechnology & Materials Science
Optics & Photonics
Impedance Analysis
Scanning Probe Microscopy
Sensors
Failure Analysis & Semiconductors

Unlock the Full Spectrum.
From DC to 8.5 GHz.
Your Application. Measured.
Find out more
Zurich Instruments

AIP Publishing

The Journal of Chemical Physics ARTICLE pubs.aip.org/aip/jcp

Valence shell electronically excited states of norbornadiene and quadricyclane

Cite as: J. Chem. Phys. 160, 064305 (2024); doi: 10.1063/5.0187707
Submitted: 15 November 2023 • Accepted: 15 January 2024 •
Published Online: 13 February 2024

View Online Export Citation CrossMark

Joseph C. Cooper,[1] David M. P. Holland,[2,a)] Rebecca A. Ingle,[3] Matteo Bonanomi,[4,5] Davide Facciala,[4] Nelson De Oliveira,[6] Abdul R. Abid,[7,8] Julien Bachmann,[9] Surjendu Bhattacharyya,[7] Kurtis Borne,[7] Michael Bosch,[9] Martin Centurion,[10] Keyu Chen,[7] Ruaridh J. G. Forbes,[11] Huynh V. S. Lam,[7] Asami Odate,[12] Artem Rudenko,[7] Anbu S. Venkatachalam,[7] Caterina Vozzi,[4] Enliang Wang,[7,13] Peter M. Weber,[12] Michael N. R. Ashfold,[14] Adam Kirrander,[1,b)] and Daniel Rolles[7,c)]

AFFILIATIONS

[1]Physical and Theoretical Chemistry Laboratory, Department of Chemistry, University of Oxford, Oxford OX1 3QZ, United Kingdom
[2]STFC, Daresbury Laboratory, Warrington WA4 2DS, United Kingdom
[3]Department of Chemistry, University College London, 20 Gordon Street, London WC1H 0AJ, United Kingdom
[4]Istituto di Fotonica e Nanotecnologie—CNR (CNR-IFN), Milano, Italy
[5]Dipartimento di Fisica, Politecnico di Milano, Italy
[6]Synchrotron Soleil, L'Orme des Merisiers, F-91192 Gif-sur-Yvette, France
[7]J. R. Macdonald Laboratory, Department of Physics, Kansas State University, Manhattan, Kansas 66506, USA
[8]Nano and Molecular Systems Research Unit, University of Oulu, 90570 Oulu, Finland
[9]Chemistry of Thin Film Materials, Friedrich-Alexander-Universität Erlangen-Nürnberg, Erlangen, Germany
[10]Department of Physics and Astronomy, University of Nebraska-Lincoln, Lincoln, Nebraska 68588, USA
[11]Linac Coherent Light Source, SLAC National Accelerator Laboratory, Menlo Park, California 94025, USA
[12]Department of Chemistry, Brown University, Providence, Rhode Island 02912, USA
[13]Hefei National Research Center for Physical Sciences at the Microscale and Department of Modern Physics, University of Science and Technology of China, Hefei 230026, China
[14]School of Chemistry, Cantock's Close University of Bristol, Bristol BS8 1TS, United Kingdom

[a)]**Author to whom correspondence should be addressed:** david.holland@stfc.ac.uk
[b)]**Electronic mail:** adam.kirrander@chem.ox.ac.uk
[c)]**Electronic mail:** rolles@phys.ksu.edu

ABSTRACT

The absolute photoabsorption cross sections of norbornadiene (NBD) and quadricyclane (QC), two isomers with chemical formula C_7H_8 that are attracting much interest for solar energy storage applications, have been measured from threshold up to 10.8 eV using the Fourier transform spectrometer at the SOLEIL synchrotron radiation facility. The absorption spectrum of NBD exhibits some sharp structure associated with transitions into Rydberg states, superimposed on several broad bands attributable to valence excitations. Sharp structure, although less pronounced, also appears in the absorption spectrum of QC. Assignments have been proposed for some of the absorption bands using calculated vertical transition energies and oscillator strengths for the electronically excited states of NBD and QC. Natural transition orbitals indicate that some of the electronically excited states in NBD have a mixed Rydberg/valence character, whereas the first ten excited singlet states in QC are all predominantly Rydberg in the vertical region. In NBD, a comparison between the vibrational structure observed in the experimental 1^1B_1–1^1A_1 ($3sa_1 \leftarrow 5b_1$) band and that predicted by Franck–Condon and Herzberg–Teller modeling has necessitated a revision of the band origin and of the vibrational assignments proposed previously. Similar comparisons have encouraged a revision of the adiabatic first ionization energy of NBD. Simulations of the vibrational structure due to excitation from the $5b_2$ orbital in QC into 3p and

28 February 2025 10:38:23

© Author(s) 2024

3d Rydberg states have allowed tentative assignments to be proposed for the complex structure observed in the absorption bands between ~5.4 and 7.0 eV.

© 2024 Author(s). All article content, except where otherwise noted, is licensed under a Creative Commons Attribution (CC BY) license (http://creativecommons.org/licenses/by/4.0/). https://doi.org/10.1063/5.0187707

I. INTRODUCTION

The valence shell electronic structure of norbornadiene (NBD) has been studied extensively, while that of quadricyclane (QC) has received much less attention. NBD and QC are isomers, with chemical formula C_7H_8 (both with C_{2v} equilibrium geometries as shown in Fig. 1), and much of the extensive current interest in these two isomers stems from the potential use of NBD/QC systems (and their derivatives) for energy storage[1–3] and photoswitches.[4] These two isomers also provide interesting comparators in the context of molecular structure and bonding. The more stable bicyclic isomer, NBD, contains two C=C double bonds and many of the early spectroscopic and theoretical studies of this molecule focused on the symmetries and energetic ordering of the highest occupied and the two lowest unoccupied π-orbitals in the ground state molecule and the relative contributions from $\pi^* \leftarrow \pi$ vs Rydberg $\leftarrow \pi$ excitations to its ultraviolet (UV) absorption. The less stable and more highly strained multi-cyclic isomer, QC, in contrast, contains only C–C and C–H single bonds and, as in the case of other closed shell alkanes (e.g., methane, ethane, cycloalkanes),[5–7] its UV absorption spectrum is dominated by excitations to Rydberg states.

The interaction between the two formally unconjugated ethylenic chromophores in NBD has been discussed[8,9] in terms of through-space (and to a much lesser extent) through-bond interactions. These interactions split the degenerate π- (and π^*-) orbitals associated with the isolated ethylenic units into symmetric and antisymmetric combinations. Upon ring closure (i.e., QC formation), these π and π^* orbitals transform into new pairs of σ and σ^* orbitals.

Given the axis system shown in Fig. 1, with the crowning CH_2 group in both isomers lying in the xz plane and the z-axis bisecting the HCH angle, the outer valence molecular orbital sequences for ground (1^1A_1) state NBD and QC are as follows:

NBD: . . .$2a_2$ $4b_2$ $7a_1(\pi_1)$ $5b_1(\pi_2)$ $5b_2(\pi_3{}^*)$ $3a_2(\pi_4{}^*)$,

QC: . . .$7a_1$ $4b_1$ $2a_2(\sigma_1)$ $5b_2(\sigma_2)$ $5b_1(\sigma_3{}^*)$ $8a_1(\sigma_4{}^*)$.

The highest occupied and lowest unoccupied valence orbitals are shown in Fig. S1 in the supplementary material but, as noted above and in more detail later, excitations to these antibonding valence orbitals in QC will be high energy transitions in the vertical region.

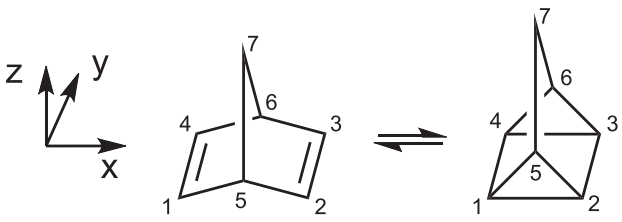

FIG. 1. A schematic showing the geometric structures of norbornadiene (left) and quadricyclane (right), and the Cartesian coordinate system used in the text and in the calculations. The numbering of the carbon atoms is marked but, for simplicity, the hydrogen atoms are not shown.

The UV absorption spectrum of NBD, first recorded in the work of Wilcox *et al.*,[10] was further studied by Robin and Kuebler[11,12] using conventional, laboratory-based, continuum sources. The latter spectrum, encompassing the energy range ~5.4 to 7.4 eV, revealed extended vibrational progressions superimposed upon several broad bands. A subsequent investigation, involving single photon absorption and polarization-dependent (2 + 1) resonance-enhanced multiphoton ionization (REMPI) experiments of both static and jet-cooled NBD enabled the vibrational structure to be studied in much greater detail.[13,14] Moreover, the polarization-dependent REMPI studies offered new insights into the symmetries of these various transitions and enabled investigation of additional, one-photon forbidden transitions. The results from these studies allowed assignments to be proposed for many of the vibrational progressions. More recently, synchrotron radiation has been employed to record the absolute photoabsorption cross section of NBD up to an energy of ~10.8 eV.[15] Much of the observed structure was assigned using calculated adiabatic and vertical excitation energies and accompanying Franck–Condon and Herzberg–Teller calculations.

The valence shell excited states of NBD have also been investigated using electron impact spectroscopy.[16–19] By measuring the spectra as a function of electron scattering angle and incident energy, the optically allowed or forbidden character of the various electronic transitions could be determined while also distinguishing between the valence and Rydberg nature of the excited state. The electron momentum distributions[19] provided additional information concerning shake-up states.

Photoelectron spectroscopy employing HeI,[20–22] HeII,[23] and synchrotron[24] radiation has enabled the valence shell ionic states of NBD to be studied and the adiabatic and vertical ionization energies (IEs) to be determined. The authors of the work of Kibel *et al.*[21] have attempted to distinguish between ionization from π and σ orbitals by measuring the photoelectron angular distributions. These ionic states have been interpreted using various theoretical approaches.[19,22,24–27] The IE of NBD has also been measured using mass spectrometry.[28]

In contrast to the wealth of spectroscopic information available on the electronically excited states of NBD, similar information for QC is sparse, with the only absorption study being that recently reported in the work of Palmer *et al.*[29] The valence shell ionic states of QC have been studied using HeI,[30] HeII,[23] and synchrotron[24] radiation, and a value for the IE has been determined with mass spectrometry.[28] The authors of the work of Martin *et al.*[30] also established that the symmetry of the highest occupied molecular orbital (HOMO) in QC was different from that in NBD by measuring the HeI excited photoelectron spectra of bare QC and of

28 February 2025 10:38:23

© Author(s) 2024

3-methylidene-quadricyclane and by comparing the bands observed in these spectra in the 8–11 eV energy range with those in the same energy range in NBD.

A reinvestigation and more detailed interpretation of the valence electronic structure of NBD and QC are particularly timely in view of recent ultrafast time-resolved, pump–probe studies of the photoinduced isomerization in the QC/NBD system using a laboratory-based laser[31] or a free electron laser[32] as the probe photon source. In both experiments, the broadband UV excitation (pump) photon had an energy of ~6 eV. Hence, the new absorption spectra of QC and NBD, reported here, together with the assignments proposed for the observed features, should help identify the excited states populated in the pump process and those implicated in the subsequent photophysics.

In the present work, high-resolution, absolute photoabsorption cross sections of room temperature samples of NBD and QC have been measured using the Fourier transform spectrometer (FTS)[33,34] at the SOLEIL synchrotron radiation facility. Assignments for many of the better resolved features have been proposed using calculated vertical transition energies and oscillator strengths. Quantum defect assessments, and information regarding the Rydberg or valence nature of the excited state obtained from previous electron impact experiments, have also helped guide these assignments. Natural transition orbital (NTO) plots[35–38] indicate that many of the electronically excited states in NBD have mixed Rydberg/valence character. This mixing leads to irregularities in both the transition energies and the relative intensities of the absorption bands ascribed to Rydberg states. Excited state vibrational structure has been simulated in calculations including excitations allowed within the Franck–Condon (FC) approximation and also those appearing through Herzberg–Teller (electronic and vibrational) coupling.[39] Hot-band excitations have also been examined and shown to make discernible contributions to the room temperature spectrum of NBD. The present work results in considerable refinements to the previously proposed vibrational analysis of the first structured absorption band of NBD, a revision of the adiabatic IE of NBD, and tentative assignments for the bands attributed to transitions involving some of the lower energy Rydberg states in QC.

II. EXPERIMENTAL APPARATUS AND PROCEDURE

The absolute photoabsorption cross sections of QC and NBD were measured using the FTS, attached to the DESIRS beamline, at the SOLEIL synchrotron radiation facility. The characteristics of the beamline and spectrometer (a modified version of a Fresnel bimirror interferometer) have been reported previously,[40] so only a brief summary is given here.

The highly coherent beam of synchrotron radiation emitted by the undulator is spatially divided at the interface of two roof-shaped reflecting mirrors. One of these reflectors is fixed and the other can be translated, thereby allowing the optical path difference to be varied. The interferogram generated by the recombination of these two beams is detected with a photodiode.

Prior to entering the FTS, the photon beam passes through the sample (either QC or NBD) vapor. Two different sample configurations were used: (1) a 100 mm long windowless absorption cell with 150 mm long entrance and exit capillaries and (2) a windowed cell. In both configurations, the cell could be filled with vapor obtained from the liquid QC or NBD samples situated outside the vacuum chamber and held at room temperature. Before use, the liquid sample was subjected to several freeze–pump–thaw cycles. The windowless, flowing sample, cell was used to record the high-resolution, room temperature spectra. However, the determination of the column gas density required for the absolute cross section measurement is not straightforward with this arrangement. Thus, an absolute photoabsorption spectrum was recorded using the windowed cell, and this spectrum was then used to calibrate the spectrum recorded in the windowless cell with the same undulator settings. Details of the calibration procedure have been presented in the work of Jacovella *et al.*[41] The experimental uncertainty in the absolute photoabsorption cross sections determined in the flowing, windowless cell is estimated to be ~10%.

The center energy of the photon intensity distribution emitted by the undulator is tunable and can be selected by adjusting the magnetic field in the undulator. Interferograms were recorded for several overlapping spectral windows (undulator settings), and the composite photoabsorption spectrum was assembled from these individual spectra. All the spectra shown in this article were recorded with the windowless, flowing sample, cell. For NBD, spectra were obtained at resolutions of 0.27 and 2.13 meV (FWHM), while for QC, a resolution of 2.13 meV (FWHM) was used.

The photon energy scale, which is intrinsically linear, obtained from the Fourier transform of the interferogram, was calibrated using the absorption line due to the Kr $4p^5(^2P_{3/2})5s \leftarrow 4p^6\ ^1S_0$ transition at 10.0324 eV.[42] A small peak due to this transition appears in the spectrum and originates from the gas filter (containing krypton) used to attenuate the high harmonics produced in the undulator.

The NBD sample (97% purity) was purchased from Sigma Aldrich and used as supplied. The QC sample was synthesized by adding Michler's ketone to NBD, and irradiating the mixture at 365 nm for 48 h. The final product was checked by ^{1}H NMR spectroscopy and resulted in ~95% photoconversion of NBD to QC, without significant contamination from other products. Further information concerning the synthesis process and an NMR spectrum of the product can be found in the supplementary material (Fig. S2).

Although the residual NBD in the present QC sample was only a few percent, some weak peaks due to this contribution are evident in the "raw" spectrum of QC, plotted in Fig. S3(a). Here, we focus particular attention on the energy region between 5.5 and 6.2 eV [Fig. S3(b)]. In NBD, this energy range exhibits vibrational progressions associated with the 1^1B_1–1^1A_1 ($3sa_1 \leftarrow 5b_1$) transition. The corresponding peaks are discernible in our raw spectrum of QC. These peaks were removed by subtracting an optimal small percentage of the NBD spectrum, recorded at the same resolution, such that the structure due to NBD in the raw QC spectrum was no longer discernible in the "pure" QC spectrum plotted in Figs. S3(b) and S4.

The intensity of the broad band radiation emitted by the undulator was sufficient to cause a small amount of photodissociation in the sample vapor (QC or NBD) in the windowless cell, as evidenced by the observation of some very small but sharp peaks attributable to acetylene (formed as a photoproduct) in the spectra at energies above ~8 eV.

We considered the possible contribution of structure associated with acetylene photoproducts in the raw QC spectrum in some

28 February 2025 10:38:23

© Author(s) 2024

detail. The absolute photoabsorption spectrum of acetylene is well established,[43–45] and the absorption band producing the small peak in our pure spectrum of QC at 8.15 eV [Fig. S3(b)] has a cross section of almost 500 Mb. Figure S5(a) shows the pure spectrum of QC co-plotted with a room temperature spectrum of acetylene,[45] also recorded on the FTS at the SOLEIL facility under optical conditions similar to those used in the present experiment. Thus, the pure QC spectrum and the acetylene spectrum may be compared directly. It is evident that the structure in the low energy region of the acetylene spectrum has no counterpart in the pure QC spectrum [Figs. S5(a) and S5(b)]. Moreover, the cross section of acetylene (<0.1 Mb) in this energy range is more than three orders of magnitude smaller than that of the band at 8.15 eV, which itself produces only a small peak in the present data.

In summary, the pure spectrum of QC is considered to be free of structure associated with acetylene photoproducts at energies below 8.15 eV. Above this energy, the observed sharp (but weak) absorption features are likely to originate from acetylene.

III. COMPUTATIONAL DETAILS

A. Methods

The theoretical prediction of vibrationally resolved electronic absorption spectra requires calculation of the electronic excitation energies and transition intensities, and of the accompanying vibrational structure.

Calculations were undertaken with the algebraic diagrammatic construction (2nd order) [ADC(2)] and the Møller–Plesset perturbation theory (2nd order) (MP2) methods. These related methods afford a consistent description of the ground and excited electronic states and a balanced description of valence and Rydberg excited states in a single-reference manner. The ADC(2), MP2, and CC2 calculations were performed using the ricc2[46] program in the TURBOMOLE 7.5 package,[47] using the resolution-of-the-identity (RI) technique, to obtain vertical transition energies and oscillator strengths. All ion calculations were performed using unrestricted Hartree–Fock as a reference. All optimizations/frequency (wavenumber) calculations used the aug-cc-pVQZ basis,[48] which was found to agree well with the larger d-aug-cc-pV5Z basis and basis set extrapolated values. Benchmark calculations were performed with MS-CASPT2 and LR-CCSD, both of which gave similar results to those reported here, as illustrated in Tables SIV and SV in the supplementary material. All optimized geometries gave predominantly single-configurational ground states, generating good Hartree–Fock references for the response theory calculations. The present calculations were performed without explicit symmetry, except for the 1^1B_2 valence state of NBD, which has a C_{2v} 1st-order saddle-point geometry very close to the NBD ground state minimum. We conjecture that this saddle point has a sufficiently long lifetime to support a few vibrational oscillations in the photoexcited molecule, giving some lifetime broadened vibrational structure (as reported by Robin and Kuebler[12]). The imaginary frequency of this saddle point breaks either the C_5C_7 or the C_6C_7 bond and leads to formation of a toluene-like intermediate with significant planarization of the six-membered ring, significantly separated from the ground state NBD minimum. In order to run Franck–Condon calculations on this state, the mode was forced to be real and positive (i.e., the saddle point was assumed to be a minimum in all modes).

The excitation characters of the various vertical transitions were determined using natural transition orbitals (NTOs)[35–38] calculated using the TheoDORE package.[49] NTOs represent separable particle and hole orbital pairs, with their relative weights showing the contribution each particle/hole pair makes to any given transition. Typically, therefore, transitions with mixed character will be carried by several NTO pairs, whereas pure transitions tend toward one pair with unit weight.

Vibrational calculations were performed using the FCClasses 3.0 package,[50] using an adiabatic Hessian sum-over-states method to allow resolution of individual vibronic transitions.[51] For the QC and NBD ground states and each excited state considered, a minimum was optimized, and subsequent frequency calculations were performed, thereby creating vibrational harmonic oscillator wavefunctions (for further details, see the supplementary material). The overlap of the vibrational wavefunctions of the initial and final states was calculated and squared to give the Franck–Condon factor (FCF). Anharmonicity was not considered as it was not particularly apparent in the experimental spectra. Time-independent calculations were checked against the time-dependent method to ensure that the effects of the truncation of the sum-over-states were minimal. Transition dipole moment gradients were calculated by numerically differentiating the transition dipole moment at the ground state minimum and subsequently used in the calculation of Herzberg–Teller contributions to the 1^1B_1–1^1A_1 ($3sa_1 \leftarrow 5b_1$) transition in NBD. Theoretical "stick" spectra, generated from the calculated vibrational transition intensities and excitation energies, were convoluted with a Gaussian function to facilitate comparison between simulated band profiles and the corresponding experimental spectra. The width of the Gaussian function was chosen to optimize the comparison.

Calculations of the ground (1^2B_1) state of the NBD cation using the MP2/aug-cc-pVQZ method returned normal mode wavenumbers that (in some cases) were significantly lower than the experimental values, thus leading to a discrepancy in the Franck–Condon envelope. Using the related CC2/aug-cc-pVQZ method instead gave vibrational envelopes for the ground state ion in much better agreement with the experimental data. Tables SVI and SVII list the normal mode wavenumbers for the ground ionic states of NBD and QC, respectively, calculated using the MP2 and CC2 methods. For both molecules, the calculated wavenumber for ν_{39} shows a strong method dependence. For all other modes of QC, the calculated wavenumbers are reassuringly self-consistent (Table SVII), while, for NBD, the two methods return very similar wavenumbers for all other modes apart from ν_{12} and ν_{23} (Table SVI).

B. Vertical excitation energies and normal mode vibrational wavenumbers

Discussion of the electronic absorption spectra for NBD and QC, reported in Sec. IV, is guided by comparison with the results of the present calculations, so it is appropriate to detail these first. Calculated vertical energies and oscillator strengths for transitions from the ground state to the first 20 singlet excited states of NBD, and the first 15 singlet excited states of QC, are listed in Tables I and II, respectively. For each excited state, the principal particle/hole orbital pairs for the corresponding vertical transition are also given. As these data show, the excited states of QC in the vertical region all

28 February 2025 10:38:23

© Author(s) 2024

TABLE I. Vertical transition energies (in eV) and oscillator strengths for the electronically excited states of norbornadiene calculated using the ADC(2) method with the aug-cc-pVQZ basis.

Electronic state				Excitation 1			Excitation 2		
Symmetry	Adiabatic	Vertical transition energy (eV)	Oscillator strength	Hole	Particle	Contribution (%)	Hole	Particle	Contribution (%)
1^1A_2	S_1	5.334	0.0000	$5b_1$	$5b_2$ V	91.4			
1^1B_1	S_2	5.896	0.0189	$5b_1$	$8a_1$ 3s	90.1			
1^1B_2	S_3	6.162	0.0255	$7a_1$	$5b_2$ V	77.9	$5b_1$	$3a_2$ V	12.8
2^1A_1	S_4	6.361	0.0243	$5b_1$	$6b_1$ $3p_x$	75.1	$7a_1$	$8a_1$ 3s	17.4
2^1A_2	S_5	6.423	0.0000	$5b_1$	$6b_2$ $3p_y$	90.8			
2^1B_1	S_6	6.510	0.0012	$5b_1$	$9a_1$ $3p_z$	90.7			
2^1B_2	S_7	6.802	0.0886	$5b_1$	$4a_2$ $3d_{xy}$	80.5	$7a_1$	$5b_2$ V	10.8
3^1A_1	S_8	6.826	0.0202	$7a_1$	$8a_1$ 3s	75.3	$5b_1$	$6b_1$ $3p_x$	15.8
3^1B_1	S_9	6.947	0.0173	$5b_1$	$10a_1$ $3d_{y^2}$	85.3	$7a_1$	$6b_1$ $3p_x$	6.6
4^1A_1	S_{10}	6.983	0.0006	$5b_1$	$7b_1$ $3d_{xz}$	82.5	$7a_1$	$9a_1$ $3p_z$	9.5
3^1A_2	S_{11}	7.136	0.0000	$5b_1$	$7b_2$ $3d_{yz}$	90.9			
3^1B_2	S_{12}	7.214	0.0149	$7a_1$	$6b_2$ $3p_y$	81.5	$5b_1$	$3a_2$ V	9.7
4^1B_1	S_{13}	7.217	0.0327	$5b_1$	$11a_1$ $3d_{z^2}$	60.3	$7a_1$	$6b_1$ $3p_x$	31.2
4^1A_2	S_{14}	7.274	0.0000	$7a_1$	$3a_2$ V	88.4			
5^1A_1	S_{15}	7.362	0.0017	$7a_1$	$9a_1$ $3p_z$	81.9	$5b_1$	$7b_1$ $3d_{xz}$	9.3
5^1B_1	S_{16}	7.429	0.0098	$7a_1$	$6b_1$ $3p_x$	52.5	$5b_1$	$12a_1$ $3d_{x^2-y^2}$	38.3
4^1B_2	S_{17}	7.562	0.0878	$5b_1$	$4a_2$ $3d_{xy}$	74.5	$7a_1$	$7b_2$ $3d_{yz}$	16.2
6^1B_1	S_{18}	7.650	0.0153	$2a_2$	$5b_2$ V	85.6			
6^1A_1	S_{19}	7.766	0.0320	$7a_1$	$10a_1$ $3d_{y^2}$	83.3	$5b_1$	$10b_1$ $4f_{yx^2}$	8.3
7^1B_1	S_{20}	7.767	0.0645	$7a_1$	$7b_1$ $3d_{xz}$	64.8	$5b_1$	$14a_1$ $4f_{y^2z}$	26.8

TABLE II. Vertical transition energies (in eV) and oscillator strengths for the electronically excited states of quadricyclane calculated using the ADC(2) method with the aug-cc-pVQZ basis.

Electronic state				Excitation 1			Excitation 2		
Symmetry	Adiabatic	Vertical transition energy (eV)	Oscillator strength	Hole	Particle	Contribution (%)	Hole	Particle	Contribution (%)
1^1B_2	S_1	5.477	0.0002	$5b_2$	$8a_1$ 3s	91.1			
1^1A_2	S_2	5.814	0.0000	$5b_2$	$6b_1$ $3p_x$	91.2			
2^1A_1	S_3	5.925	0.0007	$5b_2$	$6b_2$ $3p_y$	90.7			
2^1B_2	S_4	6.019	0.0017	$5b_2$	$9a_1$ $3p_z$	91.0			
3^1B_2	S_5	6.480	0.0001	$5b_2$	$10a_1$ $3d_{y^2}$	90.9			
3^1A_1	S_6	6.534	0.0133	$5b_2$	$7b_2$ $3d_{yz}$	90.7			
1^1B_1	S_7	6.565	0.0147	$5b_2$	$4a_2$ $3d_{xy}$	90.7			
2^1A_2	S_8	6.660	0.0000	$5b_2$	$7b_1$ $3d_{xz}$	91.0			
4^1B_2	S_9	6.832	0.0114	$5b_2$	$11a_1$ $3d_{x^2-z^2}$	91.1			
3^1A_2	S_{10}	6.863	0.0000	$2a_2$	$8a_1$ 3s	88.4			
4^1A_2	S_{11}	7.102	0.0000	$5b_2$	$8b_1$ $4p_x$	90.6			
2^1B_1	S_{12}	7.142	0.0001	$4b_1$	$8a_1$ 3s	59.4	$2a_2$	$6b_2$ $3p_y$	31.9
5^1B_2	S_{13}	7.214	0.0003	$2a_2$	$6b_1$ $3p_x$	90.2			
5^1A_2	S_{14}	7.402	0.0000	$2a_2$	$9a_1$ $3p_z$	89.6			
3^1B_1	S_{15}	7.407	0.0005	$2a_2$	$6b_2$ $3p_y$	57.9	$4b_1$	$8a_1$ 3s	32.3

28 February 2025 10:38:23

© Author(s) 2024

have dominant Rydberg character; the first predominantly valence state lies much higher in energy. In contrast, the π and π* orbitals in NBD ensure that several predominantly valence excited states (labeled V in Table I) are interspersed between, and mixed with, the Rydberg states of NBD at energies within the range investigated in the present work. Note, the various Rydberg state potentials typically support two local minima—one QC-like, the other NBD-like—corresponding to the respective minima of the QC and NBD cations.[32,52]

Normal mode vibrational wavenumbers for the ground states, the excited electronic states formed by 3s ← HOMO electron promotion, and the ground state cations, of both NBD and QC, at the respective minimum energy geometries, are given in Tables III and IV. Also included in Table III are the normal mode

TABLE III. Calculated vibrational wavenumbers (cm^{-1}) of NBD in the neutral ground 1^1A_1 state, the $3sa_1$ 1^1B_1 Rydberg state, the 1^1B_2 valence state, and the ground 1^2B_1 state of the cation.

Symmetry	Mode	Ground state 1^1A_1[a]	$3sa_1$ 1^1B_1 Rydberg state[b]	1^1B_2 valence state[b]	1^2B_1 ionic state[c]
A_1	ν_1	3265.5	3212.5	3259.8	3254.2
	ν_2	3168.3	3161.1	3173.5	3212.8
	ν_3	3089.4	3071.9	3115.5	3089.5
	ν_4	1608.2	1547.2	1447.8	1519.3
	ν_5	1491.4	1474.6	1400.5	1480.4
	ν_6	1256.4	1279.6	1124.6	1278.9
	ν_7	1124.0	1117.4	1089.0	1124.0
	ν_8	960.4	1004.9	963.9	1005.2
	ν_9	903.6	917.1	738.8	914.9
	ν_{10}	784.7	829.8	602.9	839.1
	ν_{11}	747.2	772.0	496.2	772.8
	ν_{12}	427.5	394.9	245.3	383.0
A_2	ν_{13}	3239.4	3208.2	3239.7	3236.2
	ν_{14}	1297.0	1287.4	1258.4	1285.6
	ν_{15}	1267.6	1240.7	1187.0	1244.1
	ν_{16}	1138.1	1130.7	1034.9	1141.6
	ν_{17}	938.0	970.4	954.2	965.1
	ν_{18}	914.1	881.7	692.7	896.2
	ν_{19}	721.7	703.1	516.0	707.2
	ν_{20}	453.9	370.4	286.9	376.6
B_1	ν_{21}	3263.7	3211.9	3258.3	3252.6
	ν_{22}	3166.1	3160.8	3238.2	3166.9
	ν_{23}	1568.9	1421.6	1768.0	1509.7
	ν_{24}	1229.9	1168.9	1248.1	1174.4
	ν_{25}	1077.2	1079.1	1056.3	1086.8
	ν_{26}	1032.9	1001.8	978.1	1005.9
	ν_{27}	929.6	862.5	954.1	865.8
	ν_{28}	677.6	717.6	566.8	720.3
	ν_{29}	505.9	449.5	454.9	449.7
B_2	ν_{30}	3240.1	3205.9	3238.2	3237.7
	ν_{31}	3165.8	3174.8	3172.7	3211.5
	ν_{32}	1341.4	1360.3	1307.2	1360.2
	ν_{33}	1272.4	1281.4	1127.1	1284.9
	ν_{34}	1166.5	1207.7	963.1	1206.4
	ν_{35}	975.2	1017.4	888.9	1039.9
	ν_{36}	930.7	950.6	866.8	984.4
	ν_{37}	899.3	912.0	671.7	916.1
	ν_{38}	819.4	802.0	443.1	849.1
	ν_{39}	550.7	372.3	−325.8[d]	577.4

[a]MP2 calculations.
[b]ADC(2) calculations.
[c]CC2 calculations.
[d]This negative value indicates that the 1^1B_2 state is a transition state in the near vertical region.

28 February 2025 10:38:23

© Author(s) 2024

TABLE IV. Calculated vibrational wavenumbers (cm^{-1}) of QC in the neutral ground 1^1A_1 state, the $3sa_1$ 1^1B_2 Rydberg state, and the ground 1^2B_2 state of the cation.

Symmetry	Mode	Ground state 1^1A_1[a]	$3sa_1$ 1^1B_2 Rydberg state[b]	1^2B_2 ionic state[a]
A_1	ν_1	3262.6	3201.0	3277.0
	ν_2	3230.8	3181.7	3249.8
	ν_3	3081.1	3094.7	3118.6
	ν_4	1493.3	1492.2	1494.4
	ν_5	1372.5	1451.4	1386.9
	ν_6	1282.2	1367.4	1348.7
	ν_7	1104.5	1171.6	1079.3
	ν_8	1017.7	1055.1	1061.2
	ν_9	964.7	1022.9	939.0
	ν_{10}	924.9	935.6	881.7
	ν_{11}	819.2	772.8	752.6
	ν_{12}	732.3	729.1	668.8
A_2	ν_{13}	3242.4	3198.2	3259.5
	ν_{14}	1209.2	1251.1	1253.5
	ν_{15}	1193.2	1177.5	1187.3
	ν_{16}	1047.2	1048.4	1076.9
	ν_{17}	1016.2	990.5	1004.7
	ν_{18}	852.6	812.4	825.2
	ν_{19}	710.9	625.3	632.3
	ν_{20}	532.7	382.4	389.9
B_1	ν_{21}	3252.3	3199.9	3267.5
	ν_{22}	3141.0	3175.2	3189.6
	ν_{23}	1267.8	1563.0	1330.6
	ν_{24}	1064.9	1101.4	1076.9
	ν_{25}	1011.9	1047.4	1003.5
	ν_{26}	931.2	979.9	983.4
	ν_{27}	857.7	927.3	846.2
	ν_{28}	794.5	728.7	702.0
	ν_{29}	391.1	414.9	412.2
B_2	ν_{30}	3254.6	3198.4	3267.8
	ν_{31}	3227.8	3190.4	3247.7
	ν_{32}	1387.8	1386.1	1413.0
	ν_{33}	1281.9	1272.5	1286.2
	ν_{34}	1245.0	1262.6	1265.9
	ν_{35}	1056.6	1006.9	1067.4
	ν_{36}	975.9	950.8	960.4
	ν_{37}	921.6	809.9	905.2
	ν_{38}	710.3	767.6	768.2
	ν_{39}	664.0	502.6	641.4

[a]MP2 calculations.
[b]ADC(2) calculations.

vibrational wavenumbers for the 1^1B_2 valence state in NBD. Note, in both molecules, the calculated normal mode wavenumbers for the 3s, 3p, and 3d Rydberg states are very similar (reflecting the similar topographies of the respective potential energy surfaces), so only the values for the respective 3s states are listed in Tables III and IV. The vibrational modes are numbered using the Herzberg convention.[53] The normal mode wavenumbers for the ground (1^1A_1) state neutral molecules and the associated nuclear displacements accord well with those reported previously for NBD[54,55] and QC.[56]

Comparisons between the simulated vibronic bands and the experimental spectra involved the following sequence of actions. The FC predicted intensity distribution was placed on a total energy scale by summing the theoretical adiabatic excitation energy (the separation between the minima of the ground and excited state potentials) with the vibrational energy contribution. In all cases, the simulations employed the calculated harmonic wavenumbers (Tables III and IV), except those of the absorption band due to the transition into the $3sa_1$ 1^1B_1 Rydberg state of NBD (Fig. 6 and Fig. S13) where

28 February 2025 10:38:23

© Author(s) 2024

a scaling factor of 0.94 was used. The resulting vibronic simulations matched the experiment well, apart from a (generally small) energy offset. Comparisons shown in this work are post-application of an appropriate energy shift to the simulated data, the magnitude of which is reported in the relevant figure caption. This energy offset is a consequence of the different methods used to calculate the ground and excited state electronic energies. Although comparison of absolute electronic energies between methods is not meaningful, the vibrational energy spacings and overlaps can be compared provided that the potential energy surfaces returned by the two methods are similar.

Comparisons between the vibrational simulations and the experimental spectra revealed additional transitions beyond the simple cold (0 K) Franck–Condon picture. In the case of the 3s 1^1B_1 state of NBD, Herzberg–Teller effects were considered up to first order. Additionally, the wavenumbers of several normal modes *i* of NBD are sufficiently low (see Table III) that hot-band excitations (i.e., excitations from levels with $v_i > 0$) are readily identifiable in the room temperature spectrum.

Finally in this section, we note that the $3p_x$ 1^1A_2 state in QC couples strongly with the $5b_2(\sigma_2)5b_1(\sigma_3{}^*)$ valence state upon opening of the angle between the two four-member rings (i.e., distorting toward the NBD geometry). This can be expected to preclude the observation of any associated vibrational structure (due to lifetime broadening) and to provide a route for nonadiabatic coupling back to the ground state on short timescales.[32] Excitation to the $3p_x$ 1^1A_2 state in QC is actually symmetry-forbidden at the ground state equilibrium geometry. Thus, it is shown as having zero oscillator strength in Table II. However, zero-point motion around this minimum energy geometry enables some "brightening" of the state and excitation to the $3p_x$ 1^1A_2 state in QC therefore contributes a broad featureless background absorption due to its ultrafast decay. Our analysis is primarily concerned with sharp features in the excitation spectrum of QC, to which the rapid dynamics in the valence state does not contribute. Henceforth, the 1^1A_2 state in QC will be described as the $3p_x$ Rydberg state, but it is important not to lose sight of its dynamical importance as a "doorway" for nonadiabatic coupling back to the ground state and interchange between the NBD and QC isomers.[32]

Table V provides a summary of the geometric structures of NBD and QC in three key coordinates: R_{12} (the perpendicular distance between the centers of the C_1–C_4 and C_2–C_3 bonds in Fig. 1), R_{14} [the C_1–C_4 (and C_2–C_3) bond lengths], and θ (the angle between the planes formed by the $C_1C_4C_5C_6$ and the $C_2C_3C_5C_6$ atoms). In addition, classical bond orders are provided. These are evaluated using the following formula:

$$bond\ order = \left(n_{\text{bonding}} - n_{\text{antibonding}}\right)/4,$$

where n_{bonding} and $n_{\text{antibonding}}$ are the number of bonding and antibonding electrons, respectively. In using this formula, we make the simplifying assumption that the valence orbitals only contribute to the bonding between the pairs of carbon atoms and note that the bonding is spread over two equivalent bonds. This leads to a factor of 4 in the denominator, rather than the traditional 2 used when considering the order of a bond between two atoms.

The $C_1C_4C_5C_6$ and $C_2C_3C_5C_6$ planes are well separated in the NBD ground state equilibrium geometry, as evidenced by the large R_{12} and θ values (2.46 Å and 114.7°, respectively). R_{14} is short (1.34 Å), reflecting the double bond in the respective C=C moieties. This contrasts with the ground state of QC, which has formal single bonds between the C_1 and C_2 (and C_3 and C_4) atoms; the R_{12} and R_{14} values therefore mirror typical C–C single bond values (~1.5 Å) and θ is much smaller (~62.3°) than in NBD. We note that the present values of R_{12} and R_{14} in the 1^1A_1 state of QC are very similar to the results obtained in the work of Palmer *et al.*[24] using the MP4(SDQ) approach.

TABLE V. Minimum energy geometry parameters for NBD and QC in their ground states, in selected excited states, and in the respective ground state cations. In all geometries, the C_1C_4 bond has a fully occupied sigma orbital. Formation of the 1^1B_2 S_3 state of NBD involves promoting an electron from an orbital with both C_2C_3 and C_1C_4 bonding character to an orbital with nonbonding character (with respect to these two bonds).

Molecule	State	R_{12} (Å) [bond order][a]	R_{14} (Å) [bond order][a]	θ(°)
NBD	1^1A_1 S_0	2.46 [0]	1.34 [2]	114.7
NBD	1^1B_1 S_2	2.22 [0.25]	1.37 [1.75]	100.7
NBD	1^1B_2 S_3	2.46 [0]	1.40 [1.75]	121.0
NBD	1^2B_1 ion	2.24 [0.25]	1.38 [1.75]	101.3
QC	1^1A_1 S_0	1.51 [1]	1.54 [1]	62.3
QC	2^1A_1 S_3	1.66 [0.75]	1.47 [1.25]	70.9
QC	1^2B_2 ion	1.67 [0.75]	1.47 [1.25]	71.1

[a]Bond order for the individual bonds is shown in brackets.

In both molecules, the equilibrium geometry of the 3s Rydberg state closely mirrors that of the ground state cation. In both cases, these geometries are displaced from those of the corresponding ground state neutral species with the deformation toward the other isomer. These changes can be qualitatively rationalized in terms of a simple bonding/antibonding orbital (bond order) picture. The ground state of NBD has a fully occupied HOMO (π_2), which serves as a bonding orbital between C_1 and C_4 (and C_2 and C_3) and an antibonding orbital between C_1 and C_2 (and C_3 and C_4). Removing an electron from this orbital (whether forming the 3s Rydberg state or the ground state cation) leads to a simultaneous lengthening of the C_1C_4 (and C_2C_3) bonds and a reduction of the C_1C_2 (and C_3C_4) separations. The fully occupied HOMO (σ_2) in the ground state of QC, in contrast, is a single bonding orbital between C_1 and C_2 (and C_3 and C_4) and an antibonding orbital between C_1 and C_4 (and C_2 and C_3). Removing an electron from this orbital lengthens the C_1C_2 (and C_3C_4) distances and reduces the C_1C_4 (and C_2C_3) separations.

IV. EXPERIMENTAL RESULTS AND DISCUSSION

A. Norbornadiene

1. Overview of electronic structure

The low energy end of the low-resolution (2.13 meV FWHM), absolute photoabsorption cross section of NBD is plotted in Fig. 2, together with the theoretically predicted electronically excited states using the transition energies and oscillator strengths given in Table I. Figure S6(a) shows the experimental spectrum over an extended energy range. The overall appearance of the spectrum is similar to

28 February 2025 10:38:23

© Author(s) 2024

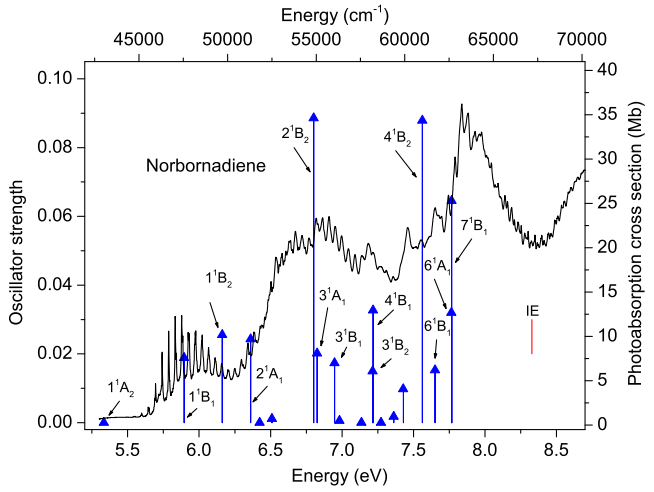

FIG. 2. The absolute photoabsorption cross section of NBD (right-hand scale). The theoretically predicted electronic transitions are plotted as vertical sticks using the calculated vertical excitation energies and oscillator strengths (left-hand scale) given in Table I. The adiabatic IE of NBD at 8.328 eV (deduced in the present work based on previous measurements,[24] see text for details) is marked.

those reported previously,[11–15] and the absolute values of the cross section are in good agreement with those presented in the work of Palmer *et al.*[15] In general, the present theoretical predictions are consistent with the earlier results presented in the work of Roos *et al.*[14]

The interpretation of the spectrum will be guided by our calculated transition energies and oscillator strengths, simulations of excited state vibrational structure using calculated vibrational wavenumbers, NTO plots enabling the Rydberg and/or valence character of the excited orbital to be visualized, and evidence from previous electron impact experiments. In addition, for absorption bands associated with Rydberg states, quantum defects will be assessed.[5] Assignments based upon quantum defect analyses work well for isolated Rydberg states. However, if a Rydberg state is perturbed through interaction with one or more adjacent states (Rydberg or valence), then the transition energy may be shifted from the value predicted using the assumed quantum defect and the oscillator strength may be perturbed. Under such circumstances, the excited state may no longer be described adequately in terms of a predominantly one-electron excited configuration but rather possesses mixed Rydberg/Rydberg or Rydberg/valence character. The NTO plots [Fig. S7(a)] generated in the present work for NBD demonstrate that Rydberg/valence mixing is significant.

The results from earlier electron impact experiments in which the scattering conditions were varied, thereby allowing an assessment of the optically allowed or forbidden nature of the transition, and the Rydberg or valence character of the final orbital, have also been used. In regard to valence transitions of NBD, Doering and McDiarmid identified two dipole-forbidden transitions at ~5.25 and ~7.50 eV, and two dipole allowed transitions at ~5.95 and ~6.65 eV.[17]

Since the geometry of a Rydberg state molecule is generally similar to that of the ionic state onto which the series converges, the FC factors connecting the ground and Rydberg states are expected to be similar to those connecting the ground and corresponding ionic state. This is particularly useful for Rydberg states belonging to series converging onto the 1^2B_1 state of the NBD cation as the photoelectron band exhibits extensive vibrational structure.[24] Moreover, as the 1^2B_1 state photoelectron band is the only band containing vibrational structure, it is a reasonable starting assumption that any Rydberg absorption band exhibiting vibrational structure is likely to correspond to a member of a series converging onto the 1^2B_1 state ionization limit.

Figure 3(a) compares the experimental 1^2B_1 state photoelectron band recorded using a room temperature sample of NBD[24] with our hot (300 K) and cold (0 K) vibrational simulations of the corresponding structure. The simulations have been obtained from the theoretical stick spectra [only the 300 K stick spectrum is shown in Fig. 3(b)] after convoluting with a Gaussian function of 20 meV

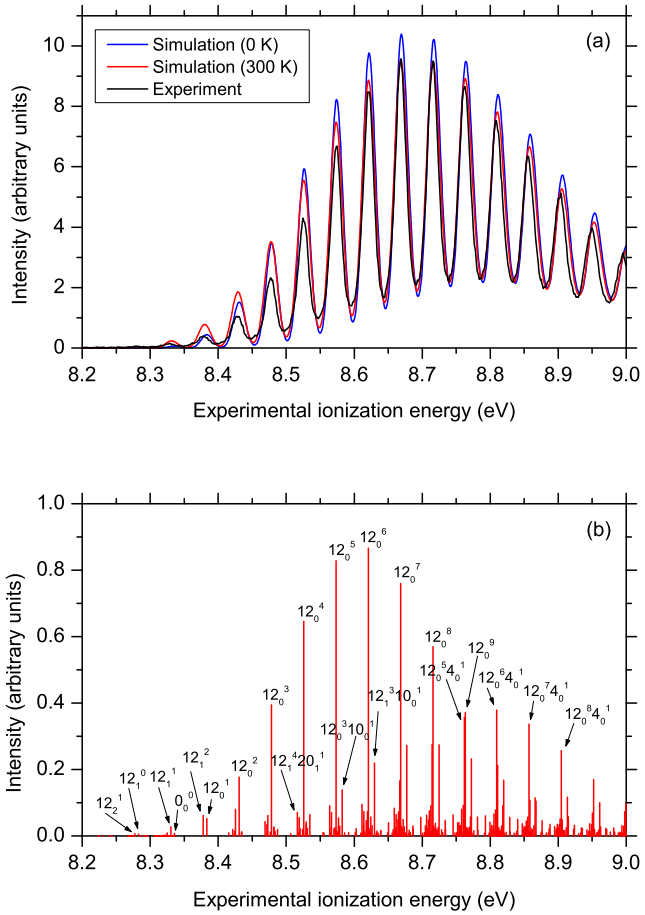

FIG. 3. (a) A comparison between the experimental 1^2B_1 state photoelectron band of NBD[24] and our hot (300 K) and cold (0 K) vibrational simulations. The simulations have been obtained from the theoretical stick spectra after convoluting with a Gaussian function of 20 meV (FWHM) to facilitate comparison with the experimental spectrum. (b) The 300 K stick spectrum, employing the calculated adiabatic ionization energy and ground and excited state vibrational wavenumbers (Table III). All calculated spectra in this figure have been shifted to higher energy by 0.299 eV so that the 12_0^8 transition aligns with the experimental peak at 8.716 eV.

28 February 2025 10:38:23

© Author(s) 2024

(FWHM) to facilitate the comparison with the experimental spectrum. The simulated spectra, employing the calculated adiabatic ionization energy and ionic ground state vibrational wavenumbers (Table III), have been shifted in energy so that the 12_0^8 transition aligns with the experimental peak at 8.716 eV. The threshold region of the photoelectron band is shown in greater detail in Fig. S8, and the hot-band excitations contributing to the peaks associated with the low vibrational levels of the cation are labeled. As reported previously, the spectrum is dominated by progressions in the lowest wavenumber totally symmetric (a_1) normal mode ν_{12} (the "wing-flapping" or "butterfly"-like C–C–C bending motion)—alone or in combination with other modes. The hot (300 K) and cold (0 K) vibrational simulations show that, contrary to a recent analysis,[24] the peak in the experimental spectrum at 8.328 eV incorporates the adiabatic transition and the peak at 8.279 eV arises solely through hot-band transitions.

In accord with previous studies,[11–18,57,58] the present calculations predict that the first excited singlet state of neutral NBD is a valence state (sometimes termed the V_1 state), arising via the optically forbidden 1^1A_2–1^1A_1 ($5b_2 \leftarrow 5b_1$) transition and with a vertical excitation energy of 5.33 eV (Table I). This conclusion is consistent with evidence from electron impact investigations,[16–18] indicating that a peak observed at ~5.25 eV should be ascribed to a singlet ← singlet, optically forbidden transition, and with the optical activity study reported in the work of Lightner *et al.*[58] The authors of the work of Palmer *et al.*[15] considered the effect of Herzberg–Teller coupling in the 1^1A_2 state and suggested that such contributions might be observable close to threshold in the absorption spectrum.

It has long been accepted that excitations into two states (one valence and the other Rydberg) occur in the energy range ~5.6 to 6.3 eV,[11–18] with the structured progression (with an average peak separation of ~45 meV, which is again attributable to FC activity in the ν_{12} mode) associated with transitions to the $3sa_1$ 1^1B_1 Rydberg state and the underlying continuum with excitation into the 1^1B_2 valence state, sometimes termed the V_2 state (Fig. 2). This coexistence was first established by Robin and Kuebler[12] and later confirmed by the authors of the work of Xing *et al.*[13] In the experiment performed by Robin and Kuebler,[12] the absorption spectrum of NBD was measured while pressurizing the cell with helium, thereby preferentially minimizing the contribution from the Rydberg state. A threshold energy of ~5.73 eV was obtained for excitation into the 1^1B_2 valence state. The authors of the work of Xing *et al.*[13] recorded the single photon absorption spectrum of NBD (which contains contributions from both Rydberg and valence transitions) and the 2 + 1 REMPI spectrum (which reports on transitions to the longer-lived Rydberg state). A simulation of the Rydberg structure was then subtracted from the one-photon absorption spectrum, leaving a broad, quasi-structureless band with an onset of 5.74 eV that was attributed to the valence state.

The 1^1B_2 valence state involves major contributions from two one-electron excitations, $5b_2 \leftarrow 7a_1$ and $3a_2 \leftarrow 5b_1$ [Fig. S7(a)], and the present calculations predict a vertical transition energy of 6.16 eV (Table I). The electron impact studies[16] associated a peak occurring at 5.95 eV with this optically allowed $\pi^* \leftarrow \pi$ transition. A comparison between the simulated vibrational structure associated with the transition into the 1^1B_2 state [employing the calculated 1^1B_2 state vibrational wavenumbers (Table III)] and the spectrum recorded by Robin and Kuebler[12] is shown in Fig. S9(a). The poorly resolved structure in the simulated spectrum, after convoluting the calculated stick spectrum (not shown) with a 40 meV FWHM Gaussian function and shifting in energy so that the features peaking at 5.73 eV align, is in good qualitative accord with the experimental data. The diffuseness of this absorption band is a clear indicator of the short-lived nature of this 1^1B_2 valence state. A non-lifetime broadened simulation of this same band (similarly shifted in energy), calculated with a resolution (~2 meV FWHM) matching that employed in the present experimental study, shows much richer structure [as shown in Fig. S9(b)]. The vibrational excitations associated with the major peaks in the spectrum plotted in Fig. S9(b) have been labeled.

The vibrational progressions appearing between 5.5 and 6.3 eV have been observed previously in single photon[11–15] and 2 + 1 REMPI[13,14] studies and associated with transitions to a single Rydberg state (the $3sa_1$ 1^1B_1 state). The authors of the work of Xing *et al.*[13] provided tentative assignments for much of the vibrational structure. These progressions are discussed in detail in Sec. IV A 2, where we show that establishing the band origin, and its energy, results in a considerable revision to earlier assignments. As a consequence of these revisions, and the anticipated envelope of the absorption band due to transitions into the 1^1B_2 valence state, all the sharp structure appearing in the experimental spectrum between ~5.5 and 6.0 eV is assigned to vibrational progressions associated with transitions into the $3sa_1$ 1^1B_1 Rydberg state, either from the zero-point (i.e. $v'' = 0$) vibrational level or from thermally populated excited vibrational levels. No evidence is found for resolved peaks associated with transitions into the 1^1B_2 valence state.

The present calculations predict vertical transition energies of 6.36 and 6.51 eV for the 2^1A_1–1^1A_1 ($3p_xb_1 \leftarrow 5b_1$) and 2^1B_1–1^1A_1 ($3p_za_1 \leftarrow 5b_1$) Rydberg excitations, respectively, with the former transition having the higher oscillator strength (Table I). The vibrational structure associated with the 1^2B_1 state photoelectron band spans a width of ~0.8 eV.[24] This is a similar width to that of the absorption band observed between 5.5 and 6.3 eV (Fig. 2). Also relevant to the interpretation of these absorption bands are the findings from the REMPI studies,[14] which suggested that the symmetry of the excited state associated with the sharp structure observed in the range 5.636–5.975 eV was B_1 or B_2, while the structure between 6.048 and 6.794 eV was associated with one or more states of A_1 symmetry.

To investigate whether the experimental evidence might be affected by the data being recorded using different techniques (one-photon absorption in the present work; two-photon absorption presented in the work of Roos *et al.*[14]), one- and two-photon excitation cross sections were calculated for excitation to some of the lower energy excited states of NBD, under various photon polarization conditions. When calculating two-photon excitation cross sections, the photon energy was set to half the transition energy (i.e., the process was treated as a one-color, two-photon excitation). The results from these calculations (Table SI) show that the two-photon excitation cross section for the $3p_x$ 2^1A_1 Rydberg state is much higher than that for the $3sa_1$ 1^1B_1 Rydberg state. Thus, the two overlapping transitions have significantly different relative transition probabilities under one- vs two-photon excitation. Note, however, that REMPI detection probabilities depend on more than just the initial multiphoton transition strengths. The ionization probability is also a

28 February 2025 10:38:23

© Author(s) 2024

sensitive function of the stability of the resonance enhancing state; shorter-lived excited states typically have a much lower ionization (and thus detection) efficiency.[59]

From here on, we focus on the one-photon absorption data. The peaks in the range ~5.5–6.4 eV (Fig. 2), generally associated with the 1^1B_1–1^1A_1 ($3sa_1 \leftarrow 5b_1$) transition, become noticeably broader and the vibrational envelope more complex as the excitation energy increases. This trend is consistent with an excited state lifetime that decreases with increasing energy, as a result of predissociation and/or anharmonic coupling to the increasing density of background vibrational levels, as suggested in the work of Xing *et al.*[13] In that study, the observed reduction in lifetime of the higher vibrational levels in the Rydberg state was attributed to a rapid depletion through coupling between the $3sa_1$ 1^1B_1 Rydberg and 1^1B_2 valence states.

The present calculations give an oscillator strength for the 2^1A_1–1^1A_1 ($3p_x \leftarrow 5b_1$) transition that is ~30% greater than that for the 1^1B_1–1^1A_1 ($3sa_1 \leftarrow 5b_1$) transition (Table I). The measured spectrum displays several short, somewhat irregular, vibrational progressions with ~45 meV peak spacings in the energy range between ~6.0 and 6.5 eV. These short progressions are not included in the extended progressions discussed in detail in Sec. IV A 2, since it is reasonable to propose that they could be attributable to transitions to the $3p_x$ 2^1A_1 state—in accord with the present theoretical predictions and the REMPI polarization results. Bearing in mind the likely vibrational envelopes of the overlapping transitions into the $3sa_1$ 1^1B_1 and $3p_x$ 2^1A_1 states (i.e., wherein the bands associated with absorption to the lowest v_{12}' levels are weak), it remains uncertain whether some of the absorption contributing to the broader peaks at energies above ~6 eV should be attributed to the $3p_x$ 2^1A_1 state rather than to the $3sa_1$ 1^1B_1 state. Excitations into the $3p_z$ 2^1B_1 state (with a predicted transition energy of 6.51 eV) might also contribute to the spectrum at the high energy end of this region, but the calculated oscillator strength for this transition (0.001) is low (Table I).

The $(7a_1)^{-1}$ 1^2A_1 state photoelectron band in NBD is structureless and has a vertical ionization energy of ~9.55 eV.[24] Assuming a quantum defect for the $3sa_1 \leftarrow 7a_1$ transition the same as that for the $3sa_1 \leftarrow 5b_1$ transition (i.e. $\delta = 0.81$) results in a predicted $3sa_1 \leftarrow 7a_1$ vertical excitation energy of 6.67 eV. The present electronic structure calculations predict that $3sa_1 \leftarrow 7a_1$ excitation contributes to both the 2^1A_1 state (at 6.36 eV) and the 3^1A_1 state (at 6.83 eV). The main particle–hole pairs [Fig. S7(a)] contributing to these two states are predicted to be the same, with the $3p_x \leftarrow 5b_1$ excitation dominating in the case of the transition to the 2^1A_1 state and the $3sa_1 \leftarrow 7a_1$ transition dominating for the 3^1A_1 state. The 2^1A_1–1^1A_1 transition may well contribute to the rise in cross section observed around 6.3 eV.

Moving to higher energies, the experimental spectrum in the energy range 6.5–7.3 eV displays at least two vibrational progressions, each with peak spacings of ~45 meV. A prominent series of fairly broad peaks, which probably belong to a single progression (P7), is observed between 6.536 and 7.184 eV (Fig. S10). Another (weaker) progression (P8) is discerned between 6.515 and 6.874 eV and a third (P9) between 6.459 and 6.639 eV. The 2^1B_2, 3^1A_1 and 3^1B_1 states are calculated to have vertical excitation energies of 6.80, 6.83, and 6.95 eV, respectively, and all have a significant oscillator strength. The 2^1B_2–1^1A_1 transition is predicted to dominate this region of the spectrum and to be carried, principally, by two one-electron promotions. The NTO plots for this state [Fig. S7(a)] show that the main contribution is associated with the $3d_{xy} \leftarrow 5b_1$ excitation, with a smaller contribution from the $5b_2 \leftarrow 7a_1$ valence excitation. The NTO plots for the 3^1B_1 state [Fig. S7(a)] also identify an excitation from the $5b_1$ orbital, namely the $3d_{y^2} \leftarrow 5b_1$ promotion, as the dominant contributor. Transitions to both the 2^1B_2 and 3^1B_1 states should thus be expected to result in absorption bands with vibrational structure resembling that in the 1^2B_1 state photoelectron band; transitions to the 2^1B_2 and 3^1B_1 states may well support the progressions observed between 6.5 and 7.3 eV. Such an interpretation appears consistent with that reached in electron impact experiments,[17] where a peak appearing at 6.65 eV, due to an optically allowed transition, was attributed to excitation into the 2^1B_2 valence state. In contrast, the dominant excitation associated with the 3^1A_1 state ($3sa_1 \leftarrow 7a_1$) may be expected to contribute a featureless band.

The calculated vertical excitation energies for the 3^1B_2 and 4^1B_1 states are very similar: 7.214 eV for 3^1B_2 and 7.217 eV for 4^1B_1. Each of the particle–hole pairs associated with the 3^1B_2 state (Table I) would be predicted to result in a structureless absorption band. For the 4^1B_1 state, the $3d_{z^2} \leftarrow 5b_1$ promotion dominates, which would be expected to support a vibrationally structured absorption band. Thus, it seems plausible that transitions into the 4^1B_1 state contribute to the structure observed between ~7.2 and 7.4 eV.

In summary, transitions from the $5b_1$ orbital into 3d Rydberg orbitals are likely to be responsible for the vibrational structure observed between ~6.4 and 7.4 eV, with the $5b_2 \leftarrow 7a_1$, $3sa_1 \leftarrow 7a_1$, $3p_y \leftarrow 7a_1$, $3a_2 \leftarrow 5b_1$, and $3p_x \leftarrow 7a_1$ excitations all potentially contributing to the underlying absorption continuum.

The present calculations give a vertical excitation energy of 7.27 eV for the (forbidden) 4^1A_2–1^1A_1 ($3a_2 \leftarrow 7a_1$) transition, which is broadly consistent with the value of 7.50 eV identified for such a dipole-forbidden transition by Doering and McDiarmid.[17]

In the energy range 7.60–8.60 eV, the experimental spectrum exhibits as least three vibrational progressions, each with a spacing of ~45 meV (Fig. S10). The first (P10), with relatively broad peaks, lies between 7.652 and 7.976 eV, the second (P11), with sharper peaks, between 8.044 and 8.325 eV, and the third (P12), also with sharp peaks, between 8.158 and 8.446 eV. The 6^1B_1–1^1A_1 ($5b_2 \leftarrow 2a_2$) valence transition is predicted at 7.65 eV, but this absorption would not be expected to display vibrational structure. On the other hand, transitions into the 4^1B_2 state (with a predicted vertical excitation energy of 7.56 eV) and into the 6^1A_1 and 7^1B_1 states (both predicted at 7.77 eV) might be expected to produce absorption bands with such vibrational spacings, since the NTO calculations show that excitations from the $5b_1$ orbital contribute to each. The broad intense peak around 7.9 eV probably arises from transitions to one or more of the 5^1A_1, 6^1A_1, and 7^1B_1 states, each of which is predicted to have a substantial oscillator strength and to be dominated by electron promotions that should give rise to structureless absorptions.

2. Vibrational progressions associated with the 1^1B_1–1^1A_1 ($3sa_1 \leftarrow 5b_1$) transition

Our high-resolution (0.27 meV FWHM) photoabsorption spectrum of NBD, covering the energy range 5.5–6.3 eV, is plotted in Fig. 4. Six progressions, all associated with the 1^1B_1–1^1A_1 ($3sa_1 \leftarrow 5b_1$) transition, are labeled (P1–P6) and color coded. These

28 February 2025 10:38:23

© Author(s) 2024

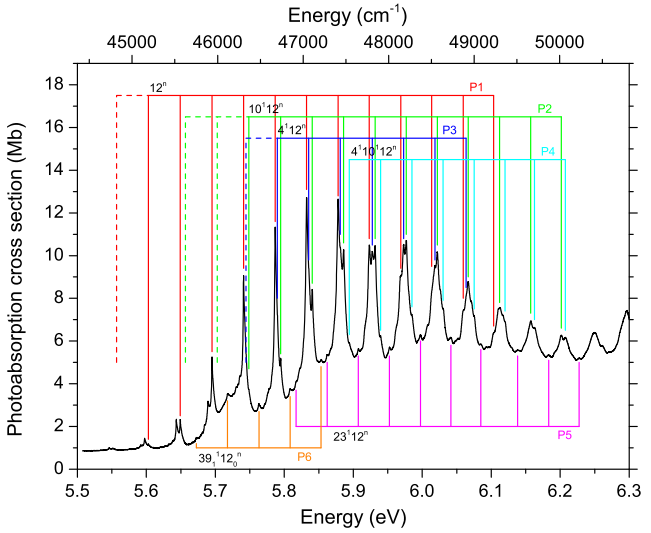

FIG. 4. The absolute photoabsorption cross section of NBD in the energy range encompassing vibrational structure due to the 1^1B_1–1^1A_1 ($3sa_1 \leftarrow 5b_1$) transition. The six identified progressions (P1–P6) are shown in greater detail in Figs. S11 and S12, and the full transition assignments (with the n values specified) and excitation energies are given in Table SII. The estimated positions for the origins of progressions P1, P2, and P3 are marked with dashed lines.

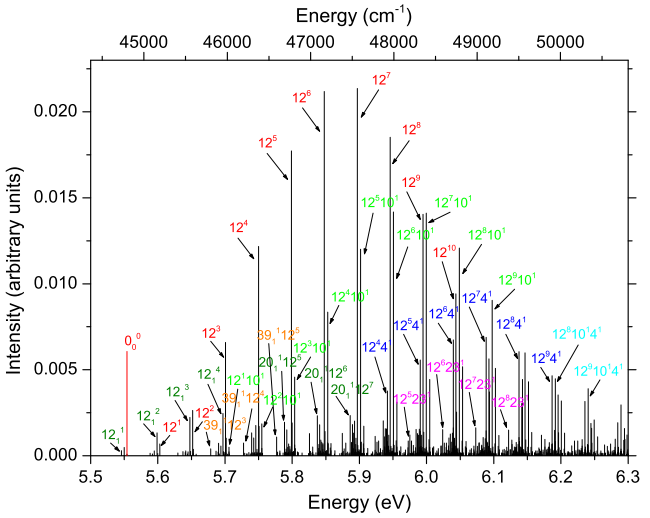

FIG. 5. Simulation of the vibrational structure associated with the 1^1B_1–1^1A_1 transition in NBD in the form of a stick spectrum. Only the stronger vibrational excitations have been labeled, and only transitions stronger than the 0_0^0 transition have been plotted. The calculated excitation energies have been shifted to higher energy by 0.1349 eV so that the energy for the 12_0^1 excitation coincides with the experimental value of 5.6029 eV. The spectrum employs the calculated vibrational wavenumbers (Table III). For display purposes, the intensity of the stick representing the 0_0^0 (origin) excitation has been multiplied by a factor of 50 and plotted in red.

progressions are shown in greater detail, together with the vibrational assignments, in Figs. S11 and S12 and the excitation energies are listed in Table SII. The predicted vibrational structure associated with the 1^1B_1–1^1A_1 transition, in the form of a stick spectrum, is plotted in Fig. 5, where only the stronger vibrational excitations are labeled. The simulation includes Herzberg–Teller coupling. The very good agreement between the simulated (Fig. S13) and observed structure allows the bands in the experimental spectrum to be assigned.

As discussed in previous studies,[11–15] the progressions associated with the 1^1B_1–1^1A_1 ($3sa_1 \leftarrow 5b_1$) transition involve excitation of ν_{12}, the wing-flapping mode, either alone or in combination with other modes. The first step in unraveling the vibrational assignments comes from comparing (Fig. 6) the present experimental spectrum and a simulation for the 1^1B_1–1^1A_1 transition at 0 K (i.e., with all ground state molecules in their $v'' = 0$ level). The origin (0_0^0) band is extremely weak (Fig. 6); its calculated FCF (Table SIII) is almost 500 times smaller than that of the strongest (n = 7) member of the 12_0^n progression. Unsurprisingly, therefore, when the simulated and experimental spectra are aligned (using the 12_0^6 band as the reference), the theoretically predicted origin band is too weak to be discerned in the room temperature absorption spectrum. The peak observed at 5.6029 eV actually corresponds to the 12_0^1 member of progression P1. Thus, our experimentally determined energy for the (unobserved) origin band is 5.5567 eV, assuming that the energetic spacing between the 0_0^0 and 12_0^1 transitions is the same as that between the 12_0^1 and 12_0^2 transitions.

A comparison between the energies for the vibrational structure appearing in the present spectrum recorded on the FTS and those for the corresponding structure reported in the work of Xing *et al.*[13]

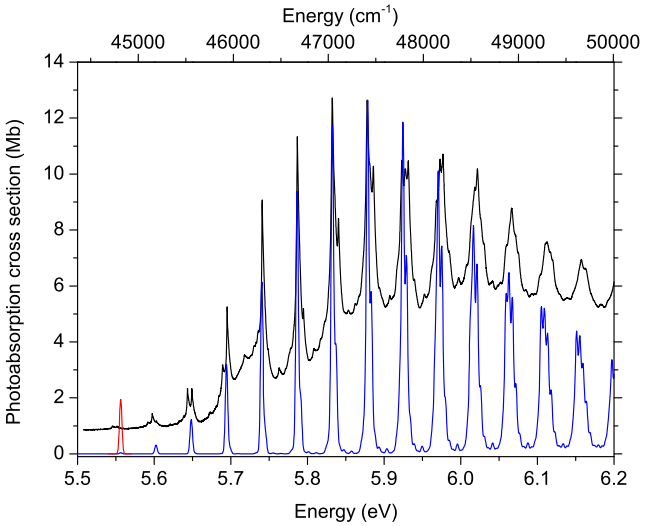

FIG. 6. Comparison between the experimental (black trace) and simulated vibrational structure, obtained from the calculated stick spectrum by convoluting with a 4 meV FWHM Gaussian function, associated with the transition to the $3sa_1$ 1^1B_1 Rydberg state of NBD. The main simulation (blue) is for a 0 K sample (i.e., all molecules initially in the $v'' = 0$ level), while the localized red trace shows the origin band re-plotted on a ×50 expanded vertical scale. The vibrational wavenumbers employed in the simulation are the calculated values (Table III), multiplied by a scaling factor of 0.94, and the simulated spectrum has been shifted to higher energy by 0.126 eV so that the peak due principally to the 12_0^6 excitation aligns with the experimental peak at 5.8323 eV.

28 February 2025 10:38:23

© Author(s) 2024

shows that the energy scale in the previously reported spectrum is offset by 8.9 meV toward higher energy. Since the energy scale in the present FTS measurements is calibrated using atomic absorption lines whose transition energies are well established, we are confident that the energy scale reported here is the correct one. We also note that the structure in the present spectrum appears to overlap very satisfactorily with that reported in the work of Palmer *et al.*[15]

Similar comparisons between the experimental spectrum and the vibrational simulations have enabled estimation of the origins for the P2 and P3 transitions, and the estimated origins for the P1, P2, and P3 progressions are marked in Fig. 4 using dashed lines.

Our vibrational simulations indicate that progressions P2 (green) and P3 (blue) involve excitation of the ν_{12} mode in combination with the excitation of a single quantum of the ν_{10} (another wing-flapping mode) or the ν_4 (C=C stretch) mode, respectively, both of which have a_1 symmetry. The experimental spectrum yields separations of 100.0 meV (806.6 cm^{-1}) and 187.6 meV (1513.1 cm^{-1}) for one quantum in the ν_{10} and ν_4 modes, respectively, in the $3sa_1$ 1^1B_1 Rydberg state. In comparison, our calculated (harmonic) energies for the ν_{10} and ν_4 modes are 102.9 and 191.8 meV (829.8 and 1547.2 cm^{-1}), respectively (Table III).

It now becomes evident, in accord with our vibrational simulation, that progression P4 (cyan) corresponds to excitation of ν_{12} in combination with a single quantum in both the ν_4 and the ν_{10} modes. Note, in contrast to the earlier study,[13] these intervals obtained in the present analysis all match well with predicted totally symmetric excited state vibrational modes. FC activity in these modes can be understood by reference to the calculated changes in equilibrium geometry upon excitation from the ground state to the $3sa_1$ 1^1B_1 Rydberg state (see Table V). Both ν_{12} and ν_{10} involve wing-flapping motions and are thus sensitive to R_{12}, which decreases upon excitation to the Rydberg state. The observed FC activity in the symmetric C=C stretch mode, ν_4, is similarly understandable given the predicted increase in R_{14} upon excitation to the Rydberg state.

The inclusion of Herzberg–Teller coupling, allowing the excitation of an odd number of quanta in non-totally symmetric vibrational modes, explains the appearance of progression P5 (magenta), which involves the excitation of ν_{12} in combination with a single quantum of the $\nu_{23}(b_1)$ mode (involving stretching of the C_1C_5, C_5C_2, C_3C_6 and C_6C_4 single bonds). The sticks corresponding to this progression are labeled in Figs. S11 and S12. Using the excitation energies of 5.9524 eV for the $23_0^1 12_0^5$ transition and 5.7868 eV for the 12_0^5 transition leads to an energy of 165.6 meV (1335.7 cm^{-1}) for one quantum of excitation in the ν_{23} mode in the $3sa_1$ 1^1B_1 Rydberg state. The calculated energy for this mode is 176.3 meV (1421.6 cm^{-1}) (Table III). Given the $^1B_1$ state symmetry, activity in this b_1 mode presumably reflects vibronic interaction with a near-resonant, optically allowed electronic state of $^1A_1$ symmetry—plausibly the 2^1A_1 state.

Next, we consider hot-band transitions. Vibrational simulations were calculated for ground state NBD molecules initially having a single quantum in the $\nu_{12}(a_1)$, $\nu_{20}(a_2$, ring twist), $\nu_{29}(b_1$, CH_2 wag), or $\nu_{39}(b_2$, ring pinching/twisting) modes. These are the lowest energy modes in each of the four symmetry species in the C_{2v} point group and are therefore the modes most likely to be thermally populated. The resulting vibrational hot-band simulations for these four modes are plotted in Fig. 7. The simulations have been shifted so that the transition energy of the band representing the 12_0^1 excitation aligns with the experimental value of 5.6029 eV. The hot-band simulation for the ν_{39} mode indicates that P6 might be attributed to the $39_1^1 12_0^n$ progression. Using the excitation energies of 5.7868 eV for the 12_0^5 transition and 5.7632 eV for the $39_1^1 12_0^5$ transition implies an energy difference of 23.6 meV between ν_{39} in the $3sa_1$ 1^1B_1 Rydberg state and in the ground (1^1A_1) state neutral. The calculated energies for the ν_{39} mode in the respective states [46.2 and 68.3 meV (372.3 and 550.7 cm^{-1}), Table III] differ by 22.1 meV, adding confidence to this hot-band assignment.

Figure 8 shows the experimental absorption spectrum of NBD near threshold. The simulated hot-band spectrum for the ν_{12} mode (Fig. 7) allows all the observed structure to be assigned. Note the absence of a peak corresponding to the origin. The excellent match between the experimental and simulated spectra after inclusion of the hot-band structure—for example, the relative intensities of the triplet feature at excitation energies of ~5.60 eV and the doublet of comparably intense features ~5.65 eV—is key to confirming the proposed numbering of the 12^n progression and thus the true energy of the (unobserved) band origin. The present analysis shows that the feature hitherto attributed to the 1^1B_1–1^1A_1 origin presented in the work of Xing *et al.*[13] and, later, Palmer *et al.*,[15] is actually the 12_0^1 transition.

As already mentioned by Robin and Kuebler,[11] the relative intensities of progressions P1–P4 vary as a function of ν_{12}', with P1 being the strongest progression for low values of ν_{12}', whereas P2 and P4 become more prominent for the higher vibrational levels (particularly evident above 6.1 eV). Our simulations indicate that a progression due to $10^2 12^n$ excitations becomes significant at energies above 6.0 eV and will contribute to the apparent broadening of the peaks associated with the higher vibrational levels. This broadening is readily observed in the experimental spectrum (Figs. S11 and S12).

B. Quadricyclane

As in the case of NBD, it proves helpful to start by considering a simulation of the vibrational structure in the 1^2B_2 state photoelectron band of QC, as these theoretical predictions help guide our interpretation of the bands in the QC photoabsorption spectrum. The simulation, shown as a stick spectrum in Fig. 9(a), has been shifted in energy so that the stick representing the $10_0^1 12_0^1$ excitation aligns with the feature at 7.858 eV in the experimental spectrum. The simulation employs the calculated vibrational wavenumbers for the 1^2B_2 ionic state given in Table IV. The present simulation is in very good accord with that reported previously in the work of Palmer *et al.*[24] and displays rich vibrational structure attributable to excitation of several a_1 symmetry normal modes. At the low energy end of the band, the structure arises primarily through excitation of two modes (ν_{10} and ν_{12}), either alone or in combination with each other. Ascending in energy, these two modes are predicted to be excited in combination with other modes, principally ν_{11}, ν_8, ν_6, and ν_5. All these modes involve (symmetric) deformation of the heavy atom skeletal modes, primarily C–C stretch and CCH bending motions.[56]

A comparison between the experimental 1^2B_2 state photoelectron band of QC, measured at a photon energy of 30 eV,[24] and a convoluted (20 meV FWHM) version of this vibrational structure is

28 February 2025 10:38:23

© Author(s) 2024

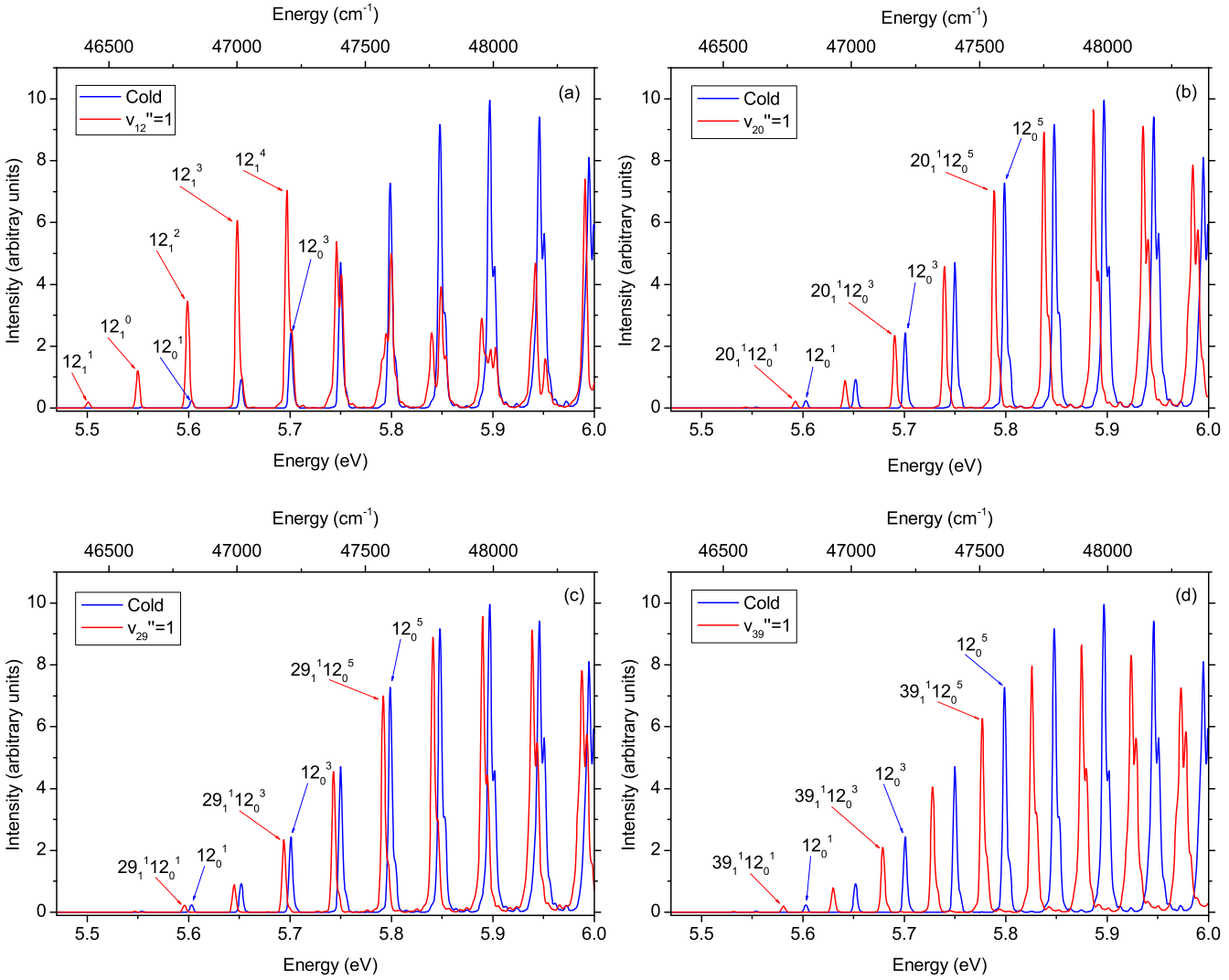

FIG. 7. Simulations of hot-band contributions associated with the dominant P1 progression in the 1^1B_1–1^1A_1 ($3sa_1 \leftarrow 5b_1$) transition of NBD. Each panel shows the dominant 12_0^n progression for a 0 K sample (in blue) and the hot-band progressions (in red) that would prevail if all the molecules were instead initially in the (a) $v_{12}'' = 1$, (b) $v_{20}'' = 1$, (c), $v_{29}'' = 1$, or (d) $v_{39}'' = 1$ levels. The simulations, obtained from the calculated stick spectra by convoluting with a 4 meV FWHM Gaussian function, have been shifted to higher energy by 0.1349 eV so that the transition energy of the band representing the 12_0^1 excitation aligns with the experimental value of 5.6029 eV.

shown in Fig. 9(b). The convoluted simulation has been shifted in energy as already described for the stick spectrum. The total width of the measured photoelectron band is almost 2 eV, with a vertical ionization energy of ~8.4 eV, but vestigial vibrational structure is only evident on the low energy side (spanning the first ~0.5 eV). The adiabatic ionization energy is 7.671 eV.[24] The peaks at the high energy side of the experimental photoelectron band (first appearing at ~8.45 eV) are due to NBD contaminant in the QC sample and can be disregarded. As previously,[24] the convoluted FC simulation reproduces the broad structures on the low energy side of the experimental photoelectron spectrum well, thereby providing confidence in the use of our current simulations to guide our interpretation of the QC photoabsorption spectrum. Only the 1^2B_2 state photoelectron band of QC exhibits any vibrational structure.[24] Hence, any features showing similar structure in the pure QC absorption spectrum are likely to be associated with Rydberg states formed through excitation from the $5b_2$ orbital.

The low energy part of the pure QC absolute photoabsorption spectrum is plotted in Fig. 10, together with the theoretically predicted excited electronic states using the transition energies and oscillator strengths given in Table II. Figure S6(b) shows the experimental spectrum over an extended energy range (up to 10.8 eV). The present calculations confirm the conclusions reached previously[3,29] that transitions to Rydberg states dominate the low energy region of

28 February 2025 10:38:23

© Author(s) 2024

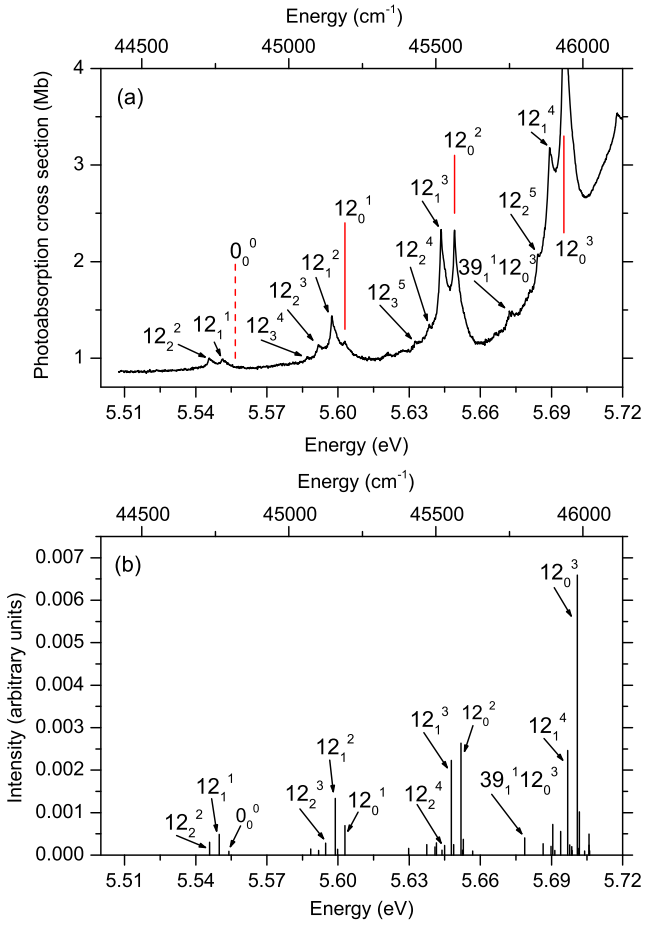

FIG. 8. (a) The absolute photoabsorption cross section of NBD in the energy region close to threshold. Peaks due to hot-band transitions are labeled as well as those associated with progression P1. A peak associated with progression P6 (the hot-band progression built on $\nu_{39}'' = 1$) is also labeled. The estimated position of the origin (0_0^0) band is marked with a dashed line. (b) A simulation, for a 300 K sample, of the vibrational structure associated with the 1^1B_1–1^1A_1 transition. The calculated excitation energies have been shifted to higher energy by 0.1349 eV so that the energy for the 12_0^1 excitation coincides with the experimental value of 5.6029 eV.

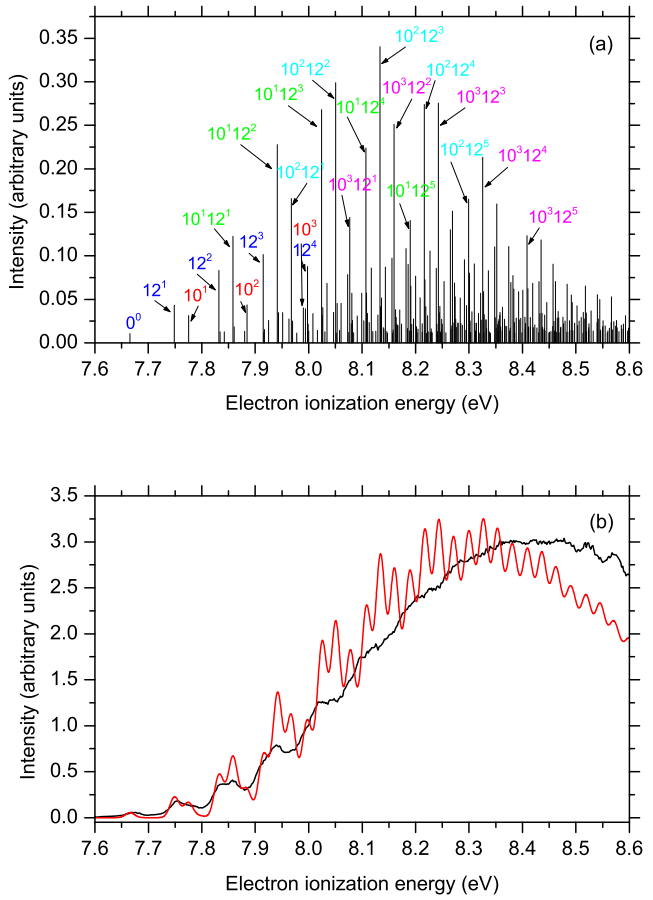

FIG. 9. (a) A stick spectrum showing the simulated vibrational structure associated with the first (1^2B_2) photoelectron band of a 300 K sample of QC. Only the stronger vibrational excitations are labeled and, since all originate from the $\nu'' = 0$ level, the subscript zero has been omitted from each label. The simulation has been shifted to lower energy by 0.057 eV so that the stick representing the $10_0^1 12_0^1$ excitation aligns with the feature at 7.858 eV in the experimental spectrum.[24] The simulation employs the calculated vibrational wavenumbers for the 1^2B_2 ionic state given in Table IV. (b) Comparison between the experimental 1^2B_2 state photoelectron band of QC[24] (black trace) and the 300 K vibrational simulation obtained by convoluting the stick spectrum shown in (a) with a 20 meV FWHM Gaussian function (red trace).

the absorption spectrum of QC (Table II). As noted in the Introduction, the saturated nature of the bonding in QC ensures that vertical excitation to states with dominant $\sigma\sigma^*$ valence character occur at substantially higher energies.

The present calculations give a vertical excitation energy of 5.48 eV for the lowest energy spin-allowed transition in QC, the 1^1B_2–1^1A_1 ($3sa_1 \leftarrow 5b_2$) excitation, and a low oscillator strength. The experimental spectrum does not exhibit a distinct threshold; the absorption cross section is seen to increase gradually from the low energy limit of the current measurements (5.4 eV). Time-resolved photoelectron spectroscopy studies[31] returned a term value (with respect to the vertical ionization limit) of 2.88 eV for the $3sa_1$ 1^1B_2 Rydberg state in QC. This corresponds to a vertical transition energy of ~5.5 eV, in good agreement with the current theoretical prediction.

Two energy ranges (5.4–6.2 eV and 6.0–6.9 eV) in the pure QC spectrum are now selected for discussion of the evident, but weak, vibrational structure. These regions encompass absorption bands associated with transitions from the $5b_2$ HOMO to, respectively, 3p and 3d Rydberg states. In both regions, the structure of interest is superimposed on substantial, energy-dependent, continuous background absorption. To highlight the vibrational structure of interest, we subtract most of the underlying continuum, resulting in the subtracted spectra plotted in Figs. 11(a) and 11(b). The subtraction was accomplished by using a smooth curve to simulate the assumed continuum background and then adjusting this curve until the subtraction of the signal under the curve from the pure QC spectrum resulted in the vibrational structure lying on a smooth, low-intensity,

28 February 2025 10:38:23

© Author(s) 2024

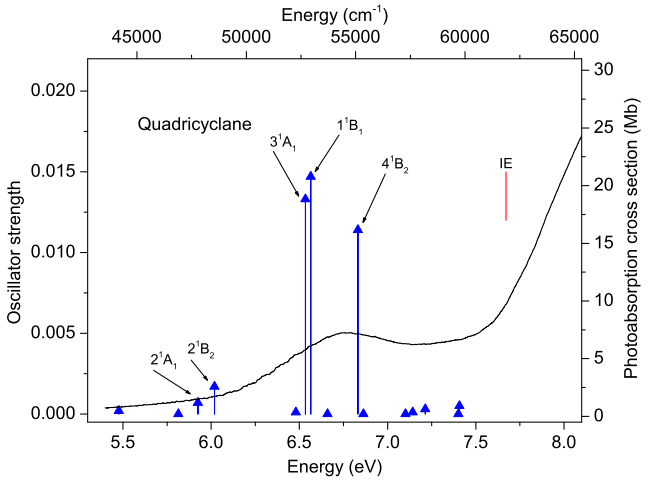

FIG. 10. The absolute photoabsorption cross section of pure QC (right hand scale). The theoretically predicted electronic transitions are plotted as vertical sticks using the calculated vertical excitation energies and oscillator strengths (left hand scale) given in Table II. The adiabatic IE of QC at 7.671 eV[24] is marked.

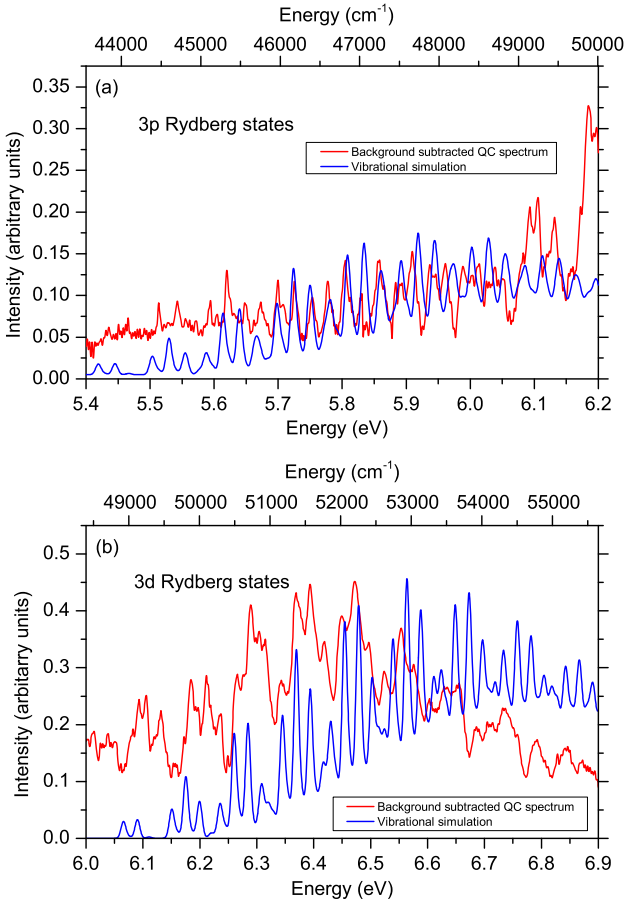

FIG. 11. The background-subtracted QC photoabsorption spectrum (red) in the energy regions predicted to encompass structure associated with transitions to (a) 3p and (b) 3d Rydberg states. FC predicted (300 K) vibrational stick spectra for excitation to, respectively, the $3p_z$ and $3d_{yz}$ orbitals, after convolution with a 10 meV FWHM Gaussian function, are plotted in blue in (a) and (b). The convoluted simulations have been shifted in energy to approximately align with the structure in the experimental data. The simulation for the 3p Rydberg state has been shifted to higher energy by 0.200 eV, while that for the 3d Rydberg state has been shifted to lower energy by 0.014 eV.

continuum. Note, our main interest in these background-subtracted spectra is the peak structure and the excitation energies, rather than the overall (slightly background dependent) profiles. Also shown in Figs. 11(a) and 11(b) are the hot (300 K) simulated vibrational stick spectra after convolution with a 10 meV FWHM Gaussian function. The simulation plotted in Fig. 11(a) is for the $3p_z \leftarrow 5b_2$ excitation, while that shown in Fig. 11(b) is for the $3d_{yz} \leftarrow 5b_2$ excitation. Both simulations use the calculated normal mode wavenumbers (Table IV) and have been chosen for further discussion as these particular excitations represent $3p \leftarrow 5b_2$ and $3d \leftarrow 5b_2$ transitions with high predicted oscillator strengths (Table II). As expected, the vibrational simulations for excitations to the $3p_y$, $3p_z$, and $3d_{yz}$ Rydberg states are all very similar and, as Figs. 11(a) and 11(b) show, the predicted structure in the convoluted simulations show reasonable agreement with that found in the experimental spectra, especially on the low energy side. The grouping of peaks into triplets [particularly in Fig. 11(b)] is noteworthy, but we also note that the alignment (in energy) between the simulations and the experimental spectra is somewhat arbitrary and that the electronic structure calculations predict that transitions to more than one Rydberg state will occur in the energy regions encompassed in both Figs. 11(a) and 11(b).

Vertical excitation energies of 5.81, 5.93, and 6.02 eV are predicted for the 1^1A_2–1^1A_1 ($3p_x \leftarrow 5b_2$), 2^1A_1–1^1A_1 ($3p_y \leftarrow 5b_2$), and 2^1B_2–1^1A_1 ($3p_z \leftarrow 5b_2$) transitions, respectively. The first of these is dipole forbidden at C_{2v} geometries but, as noted in Sec. III B, gains increasing $\sigma\sigma^*$ valence character (and thus transition probability from the ground state) upon distorting toward more NBD-like geometries.[32] This excitation can thus be expected to contribute to the underlying continuum absorption in the lower energy range. Of the other two $3p \leftarrow 5b_2$ promotions, the transition to the 2^1B_2 state is predicted to have the greater (by more than a factor of two) oscillator strength (Table II). The NTO plots [Fig. S7(b)] for the $3p_y$ 2^1A_1 and $3p_z$ 2^1B_2 states show that both are dominated by a single particle–hole orbital pair. Transitions to these Rydberg states, particularly to the $3p_z$ 2^1B_2 state, are thus most likely to account for the structure observed in the absorption spectrum between ~5.5 and 6.2 eV. For completeness, we note that excitations to the $3sa_1$ 1^1B_2 state should also be expected to contribute to the underlying continuum absorption in this energy range, but also note that the calculated oscillator strength for the 1^1B_2–1^1A_1 ($3sa_1 \leftarrow 5b_2$) transition is low.

The alignment of the simulated vibrational spectrum shown in Fig. 11(a) places it 2.33 eV below that of the 1^2B_2 state photoelectron band [Fig. 9(b)]. This energy difference implies a quantum defect of $\delta = 0.57$, which is a typical value for a p-type Rydberg state. The shift agrees well with the term values of 2.24 and 2.29 eV reported previously[31] for the two 3p states.

Vertical transition energies to five 3d Rydberg states are predicted between 6.48 and 6.83 eV (Table II). One of these (the 2^1A_2 state) is optically forbidden from the ground state and the

28 February 2025 10:38:23

© Author(s) 2024

oscillator strength for the 3^1B_2–1^1A_1 transition is low. For the remaining transitions, vertical excitation energies of 6.53 and 6.57 eV have been calculated for the 3^1A_1–1^1A_1 and 1^1B_1–1^1A_1 transitions, respectively (Table II). These two close-lying transitions are each predicted to have a high oscillator strength. At slightly higher energy, the 4^1B_2–1^1A_1 transition is predicted at 6.83 eV, with a similar oscillator strength. The NTO plots for the 3^1A_1, 1^1B_1, and 4^1B_2 states [Fig. S7(b)] show that a single particle–hole orbital pair dominates each of these states. It therefore appears reasonable to associate the vibrational structure observed in the absorption spectrum between ~6.0 and 6.8 eV with transitions to one or more of the 3^1A_1, 1^1B_1, and 4^1B_2 states, but their relative stabilities with respect to coupling to the high density of levels associated with the short-lived 3p Rydberg states (and thus the extent of their lifetime broadening) remain unknown. Again, we note that direct excitations to the 3p states are also likely to contribute to the underlying absorption continuum in this energy range.

Relative to the first photoelectron band of QC (Fig. 9), the simulated vibrational spectrum shown in Fig. 11(b) lies 1.68 eV lower in energy. This shift equates to a quantum defect of 0.15, typical for a d Rydberg state. It should be noted, however, that our calculations predict absorption to four 3d Rydberg states (three with substantial oscillator strength) in the energy range encompassed in Fig. 11(b), but only one vibrational simulation has been included in this plot. Many uncertainties thus remain with regard to any complete interpretation of the QC absorption spectrum in this energy range and at all higher energies.

Time-resolved photoelectron spectroscopy (TRPES) studies could provide one route to advancing this understanding. The first such studies, exciting QC at 208 nm (5.96 eV),[31] were interpreted (based on the observed electron kinetic energies and the derived binding energies/quantum defects) in terms of excitation to the 3s state and one or more 3p Rydberg states—consistent with the foregoing interpretation. Population in these excited states was deduced to decay on a sub-picosecond timescale. More recent TRPES studies (at 200.6 nm, 6.18 eV)[32] using an extreme UV probe wavelength (65.35 nm, equivalent to a photon energy of 18.97 eV) confirmed initial population of both 3p and 3s Rydberg states. Two sub-picosecond decay timescales were identified and interpreted via complementary *ab initio* molecular dynamics calculations. The faster process involves nonadiabatic coupling via the valence state to the ground state potential (via a conical intersection at a distorted geometry between that of QC and NBD), whereas the slower process allows some interconversion between Rydberg states of QC and NBD prior to coupling to the valence state and thence the ground state.

Further very recent TRPES studies[60] at various pump wavelengths in the range 224–195 nm (5.53–6.36 eV) provide additional support for the foregoing assignments of the UV absorption spectrum of QC, showing the (expected) increasing 3p/3s population ratio with increasing photon energy and (on the basis of deduced decay time constants) that any 3d Rydberg states populated within this photon energy range are very short lived.

V. SUMMARY

The FTS at the SOLEIL synchrotron radiation facility has been used to measure the absolute photoabsorption cross sections of NBD and QC from threshold up to 10.8 eV. Atomic absorption lines provided an accurate photon energy calibration.

The absorption spectrum of NBD exhibits some sharp structure due to transitions into Rydberg states, superimposed on several broad bands attributable to valence excitations. Some resolved, but much weaker, structure also appears in the photoabsorption spectrum of QC. Assignments have been proposed for some of the absorption bands using calculated vertical excitation energies and oscillator strengths obtained with the ADC(2) method. The character of the excited state has been investigated using NTOs, and several of the transitions in NBD have been shown to possess a mixed Rydberg/valence character.

Simulations of the excited state vibrational structure were generated from calculated transition intensities and excitation energies. These calculations include excitations allowed within the FC approximation and also those appearing through Herzberg–Teller coupling. Hot-band excitations have also been studied. Simulations of the vibrational structure associated with ionization into the 1^2B_1 state in NBD and the 1^2B_2 state in QC are consistent with the measured photoelectron spectra and proved helpful in identifying absorption bands due to transitions into Rydberg states associated with series converging onto these limits.

A comparison between the predicted vibrational structure for the 1^1B_1–1^1A_1 ($3sa_1 \leftarrow 5b_1$) transition in NBD and the experimental absorption spectrum in the energy range ~5.5 to 6.3 eV allowed the excitation energy of the origin band to be established and the active vibrational modes to be identified. Six vibrational progressions have been assigned in the 1^1B_1–1^1A_1 absorption band. Four of these progressions involve excitation to Franck–Condon active modes of a_1 symmetry. Another involves excitation of the $\nu_{23}(b_1)$ mode, enabled by Herzberg–Teller coupling, while the sixth is assigned as a hot-band progression involving the $\nu_{39}(b_2)$ mode. The present vibronic analysis reveals the need for some reassignments relative to those proposed previously.[13,15] At higher photon energies, several vibrational progressions were attributed to transitions from the HOMO into 3p or 3d Rydberg states, using calculated vertical excitation energies. The theoretical predictions also allowed several broad absorption bands to be assigned to valence excitations.

Transitions into Rydberg states dominate the energy range covered by the present absorption spectrum of QC. Weak vibrational structure, attributable to transitions from the $5b_2$ orbital into 3p or 3d Rydberg states, was observed between ~5.4 and 6.1 eV and ~6.1 to 6.8 eV, respectively. Simulations of the vibrational structure associated with the $3p_z \leftarrow 5b_2$ and $3d_{yz} \leftarrow 5b_2$ transitions were compared with the experimental spectra and some similarities were evident.

SUPPLEMENTARY MATERIAL

See the supplementary material for plots of the molecular orbitals and the NTOs of NBD and QC, a description of the synthesis of QC, figures showing the "raw" and "pure" QC absorption spectra, expanded plots of the threshold region of the 1^2B_1 state photoelectron band of NBD and the absorption spectrum of NBD (together with assignments), a discussion of one- vs two-photon excitation in NBD, a description of the benchmarking of the theoretical methods, and tables of vibrational wavenumbers.

28 February 2025 10:38:23

© Author(s) 2024

ACKNOWLEDGMENTS

The work was performed on the DESIRS beamline at the SOLEIL synchrotron radiation facility under Proposal No. 20210065. The authors are grateful to the scientific and technical staff of SOLEIL for the efficient operation of the storage ring and beamline. The authors thank Marcello Coreno (ELETTRA) for providing data files containing the photoelectron spectra of NBD and QC (measured at the GasPhase beamline) discussed in the work of Palmer *et al.* (Ref. 24) and Dr. Achim Zahl (Friedrich–Alexander University Erlangen–Nürnberg) for measuring the NMR spectrum. D.M.P.H. thanks the Science and Technology Facilities Council (United Kingdom) for financial support. J.C.C. acknowledges a doctoral studentship from the University of Oxford. A.K. acknowledges funding from the Engineering and Physical Sciences Research Council (Nos. EP/V049240/2, EP/V006819/2, EP/X026698/1, and EP/X026973/1) and the Leverhulme Trust (No. RPG-2020-208). S.B., M.C., K.C., A.R., A.K., P.M.W., and D.R. acknowledge funding by the U.S. Department of Energy, Office of Science, Basic Energy Sciences, under Award No. DE-SC0020276. K.B., H.V.S.L., and E.W. were supported by Award No. DE-FG02-86ER13491 from the same funding agency. A.O. was supported by the U.S. Department of Energy, Office of Science, Basic Energy Sciences, under Award No. DE-SC0017995. A.R.A. and A.S.V. were funded through the National Science Foundation (NSF) Grant No. PHYS-1753324. J.B. and M.B. acknowledge funding by the German Science Foundation (DFG), Grant No. 392607742.

AUTHOR DECLARATIONS

Conflict of Interest

The authors have no conflicts to disclose.

Author Contributions

Joseph C. Cooper and David M. P. Holland contributed equally to this work.

Joseph C. Cooper: Conceptualization (equal); Data curation (equal); Formal analysis (equal); Software (lead); Visualization (equal); Writing – original draft (equal); Writing – review & editing (equal). **David M. P. Holland**: Conceptualization (equal); Data curation (equal); Funding acquisition (equal); Investigation (equal); Methodology (equal); Supervision (equal); Writing – original draft (lead); Writing – review & editing (equal). **Rebecca A. Ingle**: Data curation (equal); Investigation (equal); Methodology (equal); Writing – review & editing (equal). **Matteo Bonanomi**: Data curation (equal); Investigation (equal); Methodology (equal); Writing – review & editing (equal). **Davide Faccialà**: Data curation (equal); Investigation (equal); Methodology (equal); Writing – review & editing (equal). **Nelson De Oliveira**: Data curation (equal); Formal analysis (equal); Investigation (equal); Methodology (equal); Resources (equal); Supervision (equal); Validation (equal); Writing – review & editing (equal). **Abdul R. Abid**: Data curation (equal); Investigation (equal); Methodology (equal); Writing – review & editing (equal). **Julien Bachmann**: Funding acquisition (equal); Investigation (equal); Methodology (equal); Project administration (equal); Resources (equal); Supervision (equal); Writing – review & editing (equal). **Surjendu Bhattacharyya**: Data curation (equal); Investigation (equal); Methodology (equal); Writing – review & editing (equal). **Kurtis Borne**: Data curation (equal); Investigation (equal); Methodology (equal); Writing – review & editing (equal). **Michael Bosch**: Investigation (equal); Methodology (equal); Resources (equal); Validation (equal); Writing – original draft (equal); Writing – review & editing (equal). **Martin Centurion**: Data curation (equal); Funding acquisition (equal); Project administration (equal); Writing – original draft (equal); Writing – review & editing (equal). **Keyu Chen**: Data curation (equal); Investigation (equal); Methodology (equal); Writing – review & editing (equal). **Ruaridh J. G. Forbes**: Data curation (equal); Investigation (equal); Methodology (equal); Writing – review & editing (equal). **Huynh V. S. Lam**: Data curation (equal); Investigation (equal); Methodology (equal); Writing – review & editing (equal). **Asami Odate**: Data curation (equal); Investigation (equal); Methodology (equal); Writing – review & editing (equal). **Artem Rudenko**: Data curation (equal); Funding acquisition (equal); Project administration (equal); Writing – review & editing (equal). **Anbu S. Venkatachalam**: Data curation (equal); Investigation (equal); Methodology (equal); Writing – review & editing (equal). **Caterina Vozzi**: Data curation (equal); Funding acquisition (equal); Supervision (equal); Writing – review & editing (equal). **Enliang Wang**: Data curation (equal); Investigation (equal); Methodology (equal); Writing – review & editing (equal). **Peter M. Weber**: Data curation (equal); Funding acquisition (equal); Investigation (equal); Methodology (equal); Project administration (equal); Supervision (equal); Writing – review & editing (equal). **Michael N. R. Ashfold**: Conceptualization (equal); Data curation (equal); Formal analysis (equal); Funding acquisition (equal); Investigation (equal); Methodology (equal); Supervision (equal); Validation (equal); Writing – original draft (equal); Writing – review & editing (equal). **Adam Kirrander**: Conceptualization (equal); Formal analysis (equal); Funding acquisition (equal); Project administration (equal); Software (equal); Supervision (equal); Validation (equal); Visualization (equal); Writing – original draft (equal); Writing – review & editing (equal). **Daniel Rolles**: Conceptualization (equal); Data curation (equal); Funding acquisition (equal); Investigation (equal); Methodology (equal); Project administration (equal); Supervision (equal); Writing – original draft (equal); Writing – review & editing (equal).

DATA AVAILABILITY

The data that support the findings of this study are available from the corresponding author upon reasonable request.

REFERENCES

[1] A. Dreos, K. Börjesson, Z. Wang, A. Roffey, Z. Norwood, D. Kushnir, and K. Moth-Poulsen, Energy Environ. Sci. **10**, 728 (2017).
[2] O. Brummel, F. Waidhas, U. Bauer, Y. L. Wu, S. Bochmann, H. P. Steinrück, C. Papp, J. Bachmann, and J. Libuda, J. Phys. Chem. Lett. **8**, 2819 (2017).
[3] F. Coppola, M. Nucci, M. Marazzi, D. Rocca, and M. Pastore, ChemPhotoChem **7**, e20220021 (2023).
[4] B. E. Tebikachew, F. Edhborg, N. Kann, B. Albinsson, and K. Moth-Poulsen, Phys. Chem. Chem. Phys. **20**, 23195 (2018).
[5] M. B. Robin, *Higher Excited States of Polyatomic Molecules* (Academic Press, New York, 1974), Vol. I.

28 February 2025 10:38:23

© Author(s) 2024

[6]M. B. Robin, *Higher Excited States of Polyatomic Molecules* (Academic Press, New York, 1974), Vol. II.
[7]M. B. Robin, *Higher Excited States of Polyatomic Molecules* (Academic Press, Orlando, 1985), Vol. III.
[8]R. Hoffmann, E. Heilbronner, and R. Gleiter, J. Am. Chem. Soc. **92**, 706 (1970).
[9]R. Hoffmann, Acc. Chem. Res. **4**, 1 (1971).
[10]C. F. Wilcox, S. Winstein, and W. G. McMillan, J. Am. Chem. Soc. **82**, 5450 (1960).
[11]M. B. Robin and N. A. Kuebler, J. Chem. Phys. **44**, 2664 (1966).
[12]M. B. Robin and N. A. Kuebler, J. Mol. Spectrosc. **33**, 274 (1970).
[13]X. Xing, A. Gedanken, A.-H. Sheybani, and R. McDiarmid, J. Phys. Chem. **98**, 8302 (1994).
[14]B. O. Roos, M. Merchán, R. McDiarmid, and X. Xing, J. Am. Chem. Soc. **116**, 5927 (1994).
[15]M. H. Palmer, S. V. Hoffmann, N. C. Jones, M. Coreno, M. de Simone, C. Grazioli, and R. A. Aitken, J. Chem. Phys. **155**, 034308 (2021).
[16]R. P. Frueholz, W. M. Flicker, O. A. Mosher, and A. Kuppermann, J. Chem. Phys. **70**, 1986 (1979).
[17]J. P. Doering and R. McDiarmid, J. Chem. Phys. **75**, 87 (1981).
[18]M. Allan, J. Electron Spectrosc. Relat. Phenom. **48**, 219 (1989).
[19]F. Morini, B. Hajgató, and M. S. Deleuze, J. Phys. Chem. A **114**, 9374 (2010).
[20]P. Bischof, J. A. Hashmall, E. Heilbronner, and V. Hornung, Helv. Chim. Acta **52**, 1745 (1969).
[21]M. H. Kibel, M. K. Livett, and G. L. Nyberg, J. Electron Spectrosc. Relat. Phenom. **15**, 275 (1979).
[22]K. Ohno, T. Ishida, Y. Naitoh, and Y. Izumi, J. Am. Chem. Soc. **107**, 8082 (1985).
[23]G. Bieri, F. Burger, E. Heilbronner, and J. P. Maier, Helv. Chim. Acta **60**, 2213 (1977).
[24]M. H. Palmer, M. Coreno, M. de Simone, C. Grazioli, R. A. Aitken, S. V. Hoffmann, N. C. Jones, and C. Peureux, J. Chem. Phys. **153**, 204303 (2020).
[25]E. Lindholm, C. Fridh, and L. Åsbrink, Faraday Discuss. Chem. Soc. **54**, 127 (1972).
[26]W. von Niessen and G. H. F. Diercksen, J. Electron Spectrosc. Relat. Phenom. **16**, 351 (1979).
[27]V. Galasso, Chem. Phys. **138**, 231 (1989).
[28]M. Schwell, F. Dulieu, C. Gée, H.-W. Jochims, J.-L. Chotin, H. Baumgärtel, and S. Leach, Chem. Phys. **260**, 261 (2000).
[29]M. H. Palmer, S. V. Hoffmann, N. C. Jones, M. Coreno, M. de Simone, C. Grazioli, R. A. Aitken, and C. Peureux, J. Chem. Phys. **158**, 234303 (2023).
[30]H.-D. Martin, C. Heller, E. Haselbach, and Z. Lanyjova, Helv. Chim. Acta **57**, 465 (1974).
[31]F. Rudakov and P. M. Weber, J. Chem. Phys. **136**, 134303 (2012).
[32]K. D. Borne, J. C. Cooper, M. N. R. Ashfold, J. Bachmann, S. Bhattacharyya, R. Boll, M. Bonanomi, M. Bosch, C. Callegari, M. Centurion, M. Coreno, B. F. E. Curchod, M. B. Danailov, A. Demidovich, M. Di Fraia, B. Erk, D. Faccialà, R. Feifel, R. J. G. Forbes, C. S. Hansen, D. M. P. Holland, R. A. Ingle, R. Lindh, L. Ma, H. McGhee, S. Bhavya Muvva, J. P. F. Nunes, A. Odate, S. Pathak, O. Plekan, K. C. Prince, P. Rebernik, A. Rouzée, A. Rudenko, A. Simoncig, R. J. Squibb, A. S. Venkatachalam, C. Vozzi, P. M. Weber, A. Kirrander, and D. Rolles, Nat. Chem. (2024).
[33]N. de Oliveira, D. Joyeux, D. Phalippou, J. C. Rodier, F. Polack, M. Vervloet, and L. Nahon, Rev. Sci. Instrum. **80**, 043101 (2009).
[34]N. de Oliveira, M. Roudjane, D. Joyeux, D. Phalippou, J.-C. Rodier, and L. Nahon, Nat. Photonics **5**, 149 (2011).
[35]A. V. Luzanov, A. A. Sukhorukov, and V. É. Umanskii, Theor. Exp. Chem. **10**, 354 (1976).
[36]R. L. Martin, J. Chem. Phys. **118**, 4775 (2003).
[37]F. Plasser, M. Wormit, and A. Dreuw, J. Chem. Phys. **141**, 024106 (2014).
[38]F. Plasser, S. A. Bäppler, M. Wormit, and A. Dreuw, J. Chem. Phys. **141**, 024107 (2014).
[39]G. Herzberg, *Molecular Spectra and Molecular Structure III: Electronic Spectra and Electronic Structure of Polyatomic Molecules* (Van Nostrand Reinhold, New York, 1966).
[40]L. Nahon, N. de Oliveira, G. A. Garcia, J.-F. Gil, B. Pilette, O. Marcouille, B. Lagarde, and F. Polack, J. Synchrotron Radiat. **19**, 508 (2012).
[41]U. Jacovella, D. M. P. Holland, S. Boyé-Péronne, D. Joyeux, L. E. Archer, N. de Oliveira, L. Nahon, R. R. Lucchese, H. Xu, and S. T. Pratt, J. Chem. Phys. **141**, 114303 (2014).
[42]See https://physics.nist.gov/asd for NIST Atomic Spectra Database.
[43]P. L. Smith, K. Yoshino, W. H. Parkinson, K. Ito, and G. Stark, J. Geophys. Res. **96**(E2), 17529, https://doi.org/10.1029/91je01739 (1991).
[44]Y. Bénilan, N. Smith, A. Jolly, and F. Raulin, Planet. Space Sci. **48**, 463 (2000).
[45]M. Poveda, Ph.D. thesis, Laboratoire Interuniversitaire des Systemes Atmospheriques (2023).
[46]C. Hättig, Adv. Quant. Chem. **50**, 37 (2005).
[47]*TURBOMOLE V7.5.1 2021, a development of the University of Karlsruhe and Forschungszentrum Karlsruhe, 1989–2007*, available https://www.turbomole.org.
[48]R. A. Kendall, T. H. Dunning, and R. J. Harrison, J. Chem. Phys. **96**, 6796 (1992).
[49]F. Plasser, J. Chem. Phys. **152**, 084108 (2020).
[50]J. Cerezo and F. Santoro, J. Comput. Chem. **44**, 626 (2023).
[51]F. J. Avila Ferrer and F. Santoro, Phys. Chem. Chem. Phys. **14**, 13549 (2012).
[52]I. Antol, J. Comput. Chem. **34**, 1439 (2013).
[53]G. Herzberg, *Molecular Spectra and Molecular Structure II: Infrared and Raman Spectra of Polyatomic Molecules* (van Nostrand Reinhold, New York, 1945).
[54]R. A. Shaw, C. Castro, R. Dutler, A. Rauk, and H. Wieser, J. Chem. Phys. **89**, 716 (1988).
[55]J. O. Jenson, J. Mol. Struct.: THEOCHEM **715**, 7 (2005).
[56]X. Zhou and R. Liu, Vib. Spectrosc. **12**, 65 (1996).
[57]M. Z. Zgierski and F. Zerbetto, J. Chem. Phys. **98**, 14 (1993).
[58]D. A. Lightner, J. K. Gawroński, and T. D. Bouman, J. Am. Chem. Soc. **102**, 5749 (1980).
[59]M. N. R. Ashfold, S. G. Clement, J. D. Howe, and C. M. Western, J. Chem. Soc. Faraday Trans. **89**, 1153 (1993).
[60]P. W. Weber, private communication (2024).

28 February 2025 10:38:23

© Author(s) 2024